Electrodeless plasma thrusters for spacecraft: A review

Article *in* Plasma Science and Technology · August 2017

DOI: 10.1088/2058-6272/aa71fe

3 authors, including:

Stephen Bathgate
The University of Sydney
6 PUBLICATIONS **56** CITATIONS
SEE PROFILE

Marcela Milena Marie Bilek
The University of Sydney
364 PUBLICATIONS **5,874** CITATIONS
SEE PROFILE

Electrodeless plasma thrusters for spacecraft: a review

2017 Plasma Sci. Technol. 19 083001

(http://iopscience.iop.org/1009-0630/19/8/083001)

Plasma Sci. Technol. **19** (2017) 083001 (24pp) https://doi.org/10.1088/2058-6272/aa71fe

Review

Electrodeless plasma thrusters for spacecraft: a review

S N BATHGATE[1], **M M M BILEK**[2] **and D R MCKENZIE**[2]

Applied and Plasma Physics, School of Physics, University of Sydney, NSW 2006, Australia

E-mail: stephen.bathgate@sydney.edu.au, Marcela.Bilek@sydney.edu.au and David.McKenzie@sydney.edu.au

Received 26 June 2016, revised 19 April 2017
Accepted for publication 30 April 2017
Published 20 June 2017

Abstract

The physics of electrodeless electric thrusters that use directed plasma to propel spacecraft without employing electrodes subject to plasma erosion is reviewed. Electrodeless plasma thrusters are potentially more durable than presently deployed thrusters that use electrodes such as gridded ion, Hall thrusters, arcjets and resistojets. Like other plasma thrusters, electrodeless thrusters have the advantage of reduced fuel mass compared to chemical thrusters that produce the same thrust. The status of electrodeless plasma thrusters that could be used in communications satellites and in spacecraft for interplanetary missions is examined. Electrodeless thrusters under development or planned for deployment include devices that use a rotating magnetic field; devices that use a rotating electric field; pulsed inductive devices that exploit the Lorentz force on an induced current loop in a plasma; devices that use radiofrequency fields to heat plasmas and have magnetic nozzles to accelerate the hot plasma and other devices that exploit the Lorentz force. Using metrics of specific impulse and thrust efficiency, we find that the most promising designs are those that use Lorentz forces directly to expel plasma and those that use magnetic nozzles to accelerate plasma.

Keywords: electrodeless, ion, thruster, plasma, electric, spacecraft, propulsion

(Some figures may appear in colour only in the online journal)

Nomenclature

$\mathbf{A}$	Magnetic vector potential
A_{n}	Magnetic nozzle area
$\mathbf{B}$	Magnetic flux density
B_{θ}	Azimuthal magnetic flux density
B_{m}	Magnetic mirror flux density
B_{RMF}	Rotating magnetic flux density
B_{r}	Radial magnetic flux density
B_{ω}	Rotating magnetic flux density
B_{z}	Axial magnetic flux density
c_{p}	Specific heat of a propellant at constant pressure per unit mass
δ_{s}	Resistive skin depth
ΔL	Change in circuit inductance
$\Delta\mathbf{r}(t)$	Electric field oscillating component
Δt	Orbital manoeuvre time
Δv	Velocity increment
e	Electron charge
$\mathbf{e}_B$	Magnetic field unit vector
$\mathbf{E}$	Electric field strength
$\mathbf{E}_0(\mathbf{r})$	Electric field amplitude
$E_{\max}$	Maximum amplitude of an accelerating wave field

[1] Author to whom any correspondence should be addressed.
[2] Equal senior authors.

E_{p0}	Amplitude of REF penetration into a uniform magnetized plasma
E_θ	Electric field azimuthal component
ε_a	Angular frequency ratio
ε_0	Permittivity of free space
η_p	Plasma resistivity
η_t	Thrust efficiency
F_t	Thrust
$\mathbf{F}_{pf}$	Nonlinear ponderomotive force
g_0	Acceleration due to Earth's gravity
I_{sp}	Specific impulse
$\mathbf{I}_H$	Hall current
I_c	Coil current
$\mathbf{j}$	Current density
j_z	Axial current
j_θ	Azimuthal current density
$\mathbf{j} \times \mathbf{B}$	Hall current
k_B	Boltzmann's constant
L_A	Length of an accelerating region
L_0	Initial circuit inductance
L_p	Coil length
λ_L	Laser wavelength
λ_P	Plasma wavelength
m_e	Electron mass
m_{ion}	Ion mass
$\dot{m}_p$	Rate of expulsion of propellant
m_{pl}	Payload mass
M	Mach number
μ	Dimensionless parameter
μ_m	Magnetic moment
μ_r	Relative permeability
μ_0	Magnetic permeability of free space
n_0	Initial electron number density
n_e	Electron number density
ν_{ei}	Electron–ion collision frequency
P_L	Laser power
P_s	Propulsion system power
q	Charge
r_p	Plasma radius
r	Radial position
r_m	Radius of the magnetic coil
R_{coil}	Axial coil radius
R_G	Gyration radius
R_L	Larmor radius
ρ_n	Net charge density
r_L	Radius of a laser beam spot
$\bar{\mathbf{r}}$	Time average over the oscillation period $2\pi/\omega_f$
T_c	Maximum device temperature
T_e	Electron temperature
V_B	Acceleration voltage
V_0	Initial REF voltage
$\mathbf{v}$	Ion velocity
v_e	Exhaust velocity
v_p	Propagation velocity
$v_{\|\|}$	Plasma parallel velocity
$v_\perp$	Plasma perpendicular velocity
ω_{ce}	Electron cyclotron resonant frequency
ω_{ci}	Ion cyclotron frequency
ω_f	Electromagnetic field frequency
ω_{pe0}	Initial electron plasma frequency
ω_{REF}	Rotating electric field frequency
ω_{RMF}	Rotating magnetic field frequency
Φ_{EDL}	Electric double layer potential
Ω_{ni}	Ion cyclotron frequency

1. Introduction

Electric propulsion for rockets was first proposed by the Russian physicist Konstantin Tsiolkovsky, a suggestion that had its origins in the discoveries of Thompson [1] who determined the velocities of cathode rays—now recognized as electrons—that Tsiolovsky saw were traveling 6000–20 000 times faster than the velocity of gases produced by combustion [2].

Early devices such as Space Electric Rocket Test 1, built in 1964, which was a caesium gridded ion thruster with a hollow cathode neutralizer, used electrodes that were exposed to erosion by the ionized propellant [3]. In the same year, pulsed plasma thrusters that used a 20 kA current to ablate a solid Teflon propellant were installed on the Soviet Zond-2 Mars probe and employed for attitude control [4]. Since that time a large number of devices have been tested and ion thrusters have been deployed operationally (for example Deep Space 1 [5], Dawn [6]).

To date, all deployed electric thrusters have made use of electrodes to ionize the propellant, to provide the accelerating potential for the ions and where necessary, to provide the electrons to neutralize the ions accelerated by the thruster. Although successful, the requirement for increasing power means that electrode erosion, principally by sputtering, imposes a lifetime limit on such devices. The development of electrodeless thrusters that use electric or magnetic body forces that act on ionized gases to produce a propellant stream with directed velocity is the most effective means of addressing that problem.

Among the earliest reported electrodeless plasma thrusters were the pulsed inductive thrusters developed at the aerospace corporation, TRW in the 1960s that used charge stored in a capacitor to produce a rapidly increasing current in a planar coil that ionized a propellant gas and then accelerated the resulting plasma by magnetic pressure [7]. Similar devices are still under investigation. That development was followed in the 1980s by the hybrid plume plasma rocket where plasma, confined by magnetic mirrors in a solenoidal field, was heated by radio frequency energy and accelerated by the magnetic nozzle formed in the diverging magnetic field [8]. Now known as VAriable Specific Impulse Magnetic Rocket (VASIMR), this hybrid device is undergoing durability tests that are expected to bring the device to NASA's TRL5 [9] in the near future.

Reviews and reports produced over the last 6 years [10–14] have covered various aspects of the field of electric propulsion for spacecraft. However, the rate of progress of the technology has meant that important advances, particularly in the development of electrodeless plasma thrusters, have not been adequately reviewed. Although a working spacecraft system is yet to be deployed, the field is sufficiently advanced that there is value in discussing recent progress in the design of electrodeless plasma thrusters. That is the purpose of this review.

Electrodeless plasma thrusters are here defined as devices in which energy is transferred to the propellant through the action of body forces without direct contact between the plasma and any electrode. In section 2 we describe metrics applied to plasma thrusters, in section 3 we explain the creation and acceleration of plasma relevant to electrodeless thrusters and in section 4 we describe the details of the most significant electrodeless plasma thrusters under development and demonstrate the principal advantages of such devices, namely the absence of erosion by sputtering and need to neutralize the plasma exhaust. In section 5 we summarize our findings.

2. Plasma thruster metrics

Various metrics are employed to enable comparisons to be made between thrusters that use different operating principles. Thrust is the most obvious metric although not necessarily the most informative and several other measures that relate more directly to mission requirements often have greater relevance. The most significant metrics are discussed in the following sub-sections: thrust, specific impulse, thrust efficiency and specific mass together with thruster lifetime, the advantage enjoyed by electrodeless thrusters.

2.1. Thrust F_t

Spacecraft are propelled by the directed expulsion of high velocity particles, typically in the form of a gas or plasma. According to Newton's second law, thrust is defined as the instantaneous force on a spacecraft that is proportional to the vector sum of the time rate of change of the momenta of the expelled propellant particles *i*. If the instantaneous rate of expulsion of propellant is $\dot{m}_p$ and the propellant is expelled at a velocity v_e, relative to the spacecraft, then the thrust is given by:

$$F_t = -\sum_i \dot{m}_p v_e, \tag{1}$$

where F_t is the thrust in Newtons.

2.2. Specific impulse I_{sp}

Specific impulse, I_{sp}, is usually considered to be the primary figure of merit of a thruster [14] and is defined as the value of the thrust divided by the weight of propellant expelled in unit time. Specific impulse is a measure of the capacity of a propulsion system to impart a velocity increment Δv to a spacecraft and through Tsiolkovsky's rocket equation and the exhaust velocity v_e, specific impulse largely determines the practicality of a mission.

$$I_{sp} = \frac{F_t}{\dot{m}_p\, g_0} = \frac{v_e}{g_0}(\mathrm{s}), \tag{2}$$

where g_0 is the acceleration due to gravity at Earth's surface.

An $I_{sp} \geqslant 3000$ s, corresponding to an energy of 4.5 eV per atomic mass unit of propellant, is considered to be a minimum requirement for many remote planetary missions [15].

2.3. Thrust efficiency η_t

The thrust efficiency η_t of a rocket or thruster is the secondary figure of merit and is a measure of the effectiveness of the propulsion system in converting the propellant together with the energy input (chemical, electrical or thermal) to the directed kinetic energy of the exhaust jet. Thrust efficiency is less important than specific impulse as a performance metric for electric thrusters since propellant mass rather than energy, typically produced by solar photovoltaic panels, is usually a mission's limiting factor.

$$\eta_t = \frac{\text{Directed kinetic energy in jet}}{\text{Energy from power supply}}. \tag{3}$$

2.4. Specific mass

Specific mass is given as kg kW^{-1} and is the ratio of the mass of a propulsion system (including components such as the fuel system and tanks, solar panels, power supply and the thruster itself) to the power delivered to the exhaust. Although a propulsion system may have a high specific impulse and thrust efficiency, a high specific mass will negate those advantages by reducing the proportion of the total mass of a spacecraft that can be used for payload and structures.

2.5. Trade-offs between metrics

For any mission the orbital requirements are (1) the required velocity increment Δv, (2) the time to complete an orbital manoeuvre Δt and (3) the payload mass m_{pl}. For a propulsion

Table 1. Reported lifetime of typical plasma thrusters with electrodes.

Thruster type	Power (kW)	Lifetime (h)	Reference
Gridded ion (NSTAR)	2.3	~30 000	[17]
Hall (BPT-4000)	4.5	10 400 ('zero' erosion)	[18]
Applied field magneto-plasma-dynamic	30	8000–10 000	[19]

system, the determining metrics are, thrust F_t, specific impulse I_{sp}, propulsion system power P_s and thrust efficiency η_t which can be expressed as:

$$\eta_t = \left(\frac{g_0}{2}\right)\left(\frac{F_t}{P_s}\right)I_{sp}. \tag{4}$$

While the orbital manoeuvre time can be expressed as:

$$\Delta t = \left(\frac{m_{pl}}{P_s}\right)\left(\frac{(g_0 I_{sp})^2}{2\eta_t}\right)\left(e^{\left(\frac{\Delta v}{g_0 I_{sp}}\right)} - 1\right). \tag{5}$$

These relationships between the mission parameters and those of the spacecraft propulsion system show that there is a capacity for trade-offs between the various parameters and it is possible to optimize factors such as transit time, specific impulse and payload mass for a particular mission [16].

2.6. Plasma thruster lifetime

Sputtering causes grid erosion in gridded ion thrusters, electrode erosion in magneto-plasma-dynamic thrusters, wall erosion in all types of thrusters (although magnetic shielding can greatly reduced such erosion) and erodes the cathodes used to provide the electrons that neutralize the exhaust in thrusters that produced charged ion beams. Erosion gradually degrades the performance of those devices as well as limiting their maximum lifetimes (table 1).

At the power levels presently employed in thrusters—several kilowatts—erosion has not caused serious problems but as missions that require higher power and greater thrust as well as a longer duration are conducted, grids, walls and cathodes will be exposed to more intense ion fluxes as larger masses of propellant are accelerated. Electrodeless thrusters will become more important since erosion is not the life-limiting factor in such devices.

3. Basic physics of plasma thrusters and related devices

Plasma thrusters may use electrostatic forces, as in gridded ion thrusters, magnetic forces as in magneto-plasma-dynamic thrusters or a combination of magnetic and electrostatic forces as in Hall thrusters. The mechanism of a plasma thruster involves two distinct processes: (1) the creation of the plasma and (2) its acceleration and its detachment if a magnetic nozzle is employed. These processes are discussed in the following sections.

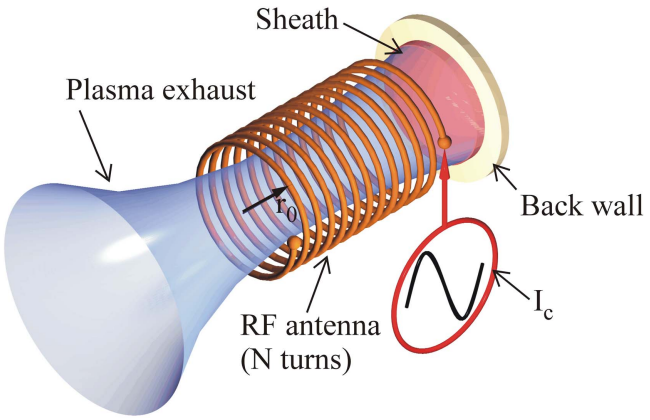

Figure 1. Simple open-ended plasma thruster showing RF antenna of N turns, input current I_c, sheath, back wall, and plasma exhaust. Thrust is produced by the reaction of the plasma through the sheath against the back wall which may be eroded by ion bombardment [20].

3.1. Plasma creation

Plasma for thrusters may be produced by a variety of mechanisms.

1. Through the effect of Faraday's law where a changing magnetic flux induces an electric field that can ionize a low-pressure gas by stripping electrons from atoms and molecules. Radio frequency energy is typically used with various kinds of antenna and this process is a useful electrodeless mechanism for producing plasma from gaseous propellants. Helicon plasma thrusters, pulsed inductive thrusters and radio frequency ion thrusters (RITs) that use grids to accelerate plasma employ this mechanism which is the most commonly used means of producing plasmas in electrodeless plasma thrusters (figure 1).
2. Electron cyclotron resonance (ECR) ion sources are electrodeless devices that produce ions by the absorption of microwave energy at the cyclotron resonant frequency in an ionized gas in a solenoidal magnetic field. When the time varying electric field of the microwaves is in phase with the gyration of the electrons at the cyclotron resonant frequency ω_{ce} in the magnetic field and orthogonal to that field then the electrons absorb energy. The energetic electrons then heat the plasma by collision [21] (figure 2). The cyclotron resonant frequency is given by:

$$\omega_{ce} = \frac{eB}{m_e}, \tag{6}$$

where e = electron charge (C), B = magnetic field strength (T) and m_e = electron mass (kg).

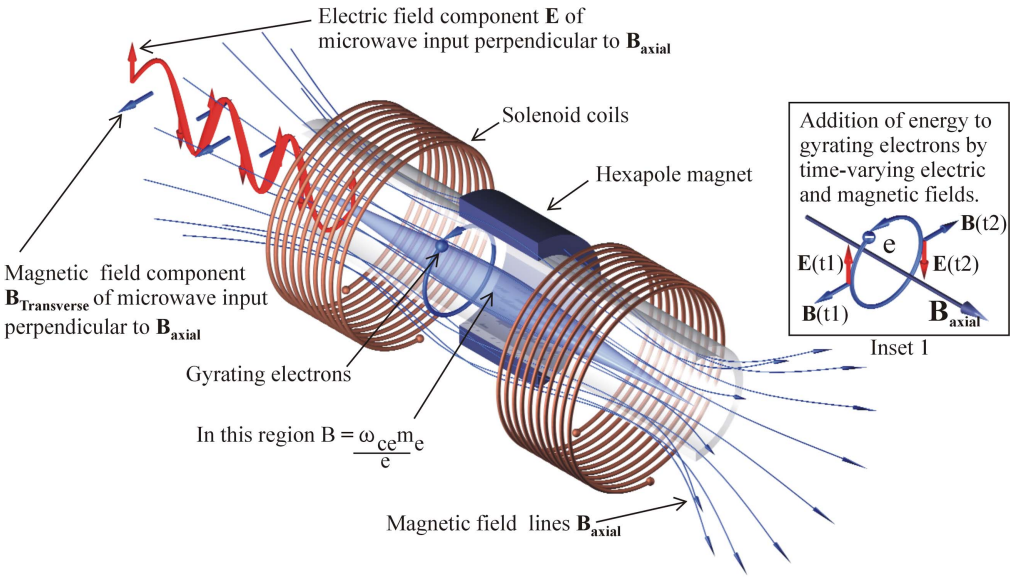

Figure 2. An electron cyclotron resonance plasma source. The electrons are heated by resonance with the time varying electric field of the microwave beam and collisions between electrons and neutrals lead to a high ionization ratio. Inset 1 shows the resonant interaction between the time-varying electric and magnetic fields of the microwave radiation and the electrons gyrating in the magnetic field. Plasma produced by this electrodeless mechanism can be accelerated by Lorentz forces in a magnetic nozzle or a traveling magnetic field.

Table 2. Principal electric thruster types employing Lorentz forces to accelerate plasmas. m_e is the electron mass (kg), ω_f is the applied field frequency (rad s^{-1}), ω_{ce} is the electron cyclotron frequency (rad s^{-1}) and E_{0z} is the electric field strength (V).

Thruster type	Accelerating force
Gridded ion, RIT thrusters and Hall thrusters.	Electrostatic attraction $\mathbf{F}_t = q\mathbf{E}$
Magnetic nozzles, magneto-plasma-dynamic thrusters, rotating electric field, theta pinch, pulsed plasma and pulsed inductive thrusters.	Magnetic fields $\mathbf{F}_t = q(\mathbf{v} \times \mathbf{B})$
Magnetized ponderomotive force thrusters (section 3.2.7)	$\mathbf{F}_{magnetized} = -\frac{q^2}{4m_e}\frac{1}{(\omega_f^2 - \omega_{ce}^2)}\frac{\partial E_{0z}^2}{\partial \bar{z}}$
Ponderomotive force thrusters (laser wake field) (section 3.2.8)	$\mathbf{F}_{unmagnetized} = \frac{-q^2}{4m_e\omega_f^2}\frac{\partial E_{0z}^2}{\partial \bar{z}}$

The electrons also collide inelastically with neutral gas atoms or molecules and that process leads to the further ionization of the gas (figure 2).

3. By a DC potential to produce a low current density discharge known as a glow discharge where plasma is produced by the bombardment of a gas by electrons and ions that are accelerated by the potential between electrodes. This mechanism may be used to produce ions for gridded ion thrusters.
4. By a high current density discharge or arc that may be initiated when the cathode becomes sufficiently hot that it emits electrons thermionically. Otherwise an arc may be initiated as a glow discharge. Magneto-plasma-dynamic, cathodic arc and electrothermal thrusters are devices with electrodes that produce ions by this means.

3.2. Plasma acceleration

Once created, plasma has to be accelerated to produce thrust. There are a number of mechanisms that can be used for this purpose, some more effective than others. The following sections describe mechanisms that have been used or proposed as a means of accelerating plasma in electrodeless thrusters.

3.2.1. Lorentz forces. Aside from any thrust that may arise from the pressure of the plasma against the thruster structure, the propulsion force or thrust $\mathbf{F}_t$ is generated in the majority of plasma thrusters by body forces that are described by the Lorentz equation:

$$\mathbf{F}_t = q\mathbf{E} + q(\mathbf{v} \times \mathbf{B}), \tag{7}$$

where q = the charge on ions, $\mathbf{E}$ = the electric field, if any, $\mathbf{v}$ = the ion velocity and $\mathbf{B}$ = the magnetic field where present that is typically produced by current in a coil.

Lorentz forces provide the acceleration of charged particles in electric thrusters by a variety of mechanisms. The principal variants that employ Lorentz forces are shown in table 2.

The theta-pinch thruster is an example of a device that uses magnetic fields to accelerate plasma. The acceleration mechanism detailed in the following analysis assumes that (1) there is a plasma present when the current starts flowing in the thruster coil and (2) that there is no magnetic field trapped in

the plasma. Given these assumptions, the plasma is driven away from the coil by an increase in magnetic pressure that arises from the $\mathbf{j} \times \mathbf{B}$ Lorentz force acting between an induced plasma current I_p and the axial magnetic field B_z. The interaction produces a magnetic pressure that compresses the plasma and a magnetic tension that together with the magnetic pressure drives the plasma from the coil. Using Ampere's law in differential form to obtain the force density exerted by the field B_z on the plasma current I_p we have:

$$\mathbf{F} = \mathbf{j} \times \mathbf{B} = (\nabla \times \mathbf{B}) \times \frac{\mathbf{B}}{\mu_0}. \tag{8}$$

Using the vector identity:

$$\frac{1}{2}\nabla(\mathbf{B} \cdot \mathbf{B}) = \mathbf{B} \times (\nabla \times \mathbf{B}) + (\mathbf{B} \cdot \nabla)\mathbf{B}. \tag{9}$$

Gives:

$$\mathbf{F} = \mathbf{j} \times \mathbf{B} = \frac{1}{\mu_0}(\mathbf{B} \cdot \nabla)\mathbf{B} - \nabla\left(\frac{B^2}{2\mu_0}\right). \tag{10}$$

The first term on the right represents a magnetic tension force[3] of magnitude $\frac{B^2}{\mu_0}$ that is parallel to $\mathbf{B}$ and the second term represents a magnetic pressure of magnitude $\frac{B^2}{2\mu_0}$ that is perpendicular to $\mathbf{B}$ and parallel to the field gradient. The process may be seen in the following example—a linear theta pinch thruster that produces a high velocity plasma jet by driving a large current of short duration through a single turn coil. If of sufficient intensity, the rapidly changing axial field B_z produced by the current pulse induces an electric field in the theta or azimuthal direction that ionizes a gas. Otherwise, a separate source of ionized gas provides the plasma propellant.

The plasma is heated and compressed by the Lorentz force produced by the increasing magnetic field and is expelled from the ends of the coil as jets (figure 3) [22].

3.2.2. Magnetic nozzles. A magnetic nozzle is formed whenever a solenoidal field is used to confine plasma and can be used to direct and accelerate plasma by interactions between the plasma and the magnetic field (figure 4). Although there are functional similarities between the operation of a conventional convergent-divergent de-Laval nozzle in a chemical rocket and a magnetic nozzle, the processes in an electric thruster can supply more energy to the propellant than is possible in a chemical rocket. In general, magnetic nozzles may be regarded as electrothermal devices where the plasma may be produced by a number of different mechanisms and magnetic and thermal forces together with ambipolar acceleration that balances an electron pressure gradient drive the plasma from the nozzle [23].

Early work [24] demonstrated that a magnetic nozzle could produce steady supersonic plasma flows with Mach

[3] Magnetic tension force acts to straighten curved magnetic field lines.

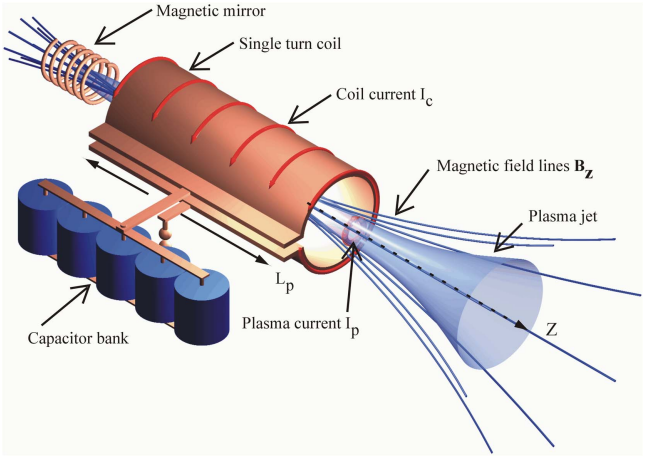

Figure 3. Linear theta pinch thruster basic configuration showing a plasma jet that is heated and compressed by the magnetic field B_z produced by a large transient current I_c from the capacitor bank that passes through a single turn coil of length L_p. A magnetic mirror may be employed to reverse the direction of the plasma jet emerging from the spacecraft end of the thruster.

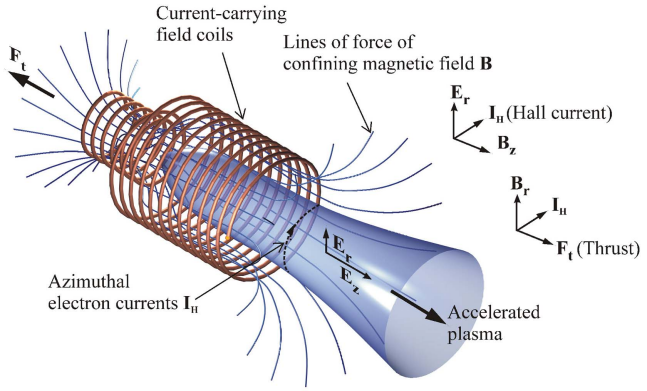

Figure 4. A magnetic nozzle showing the magnetic field strength along the axis of the nozzle. E_r and E_z are the components of the electric field that is the result of the electron pressure gradient produced by the diverging magnetic field. Currents in the field coils generate the magnetic field $\mathbf{B}$ that interacts with the electric field to produce azimuthal electron Hall currents $\mathbf{I_H}$, (produced in the $E_r \times B_z$ direction when an electric field is applied to a conductor containing a magnetic field). Those currents then create magnetic forces that accelerate the plasma and produce thrust $\mathbf{F_t}$.

numbers of the order of 3. Those experimental results showed a relation between the magnetic nozzle area $A_n(z)$, and the measured Mach number $M(z)$, both expressed as a function of distance z along the nozzle in accordance with the fluid equation for isothermal ions and electrons:

$$\frac{M^2 - 1}{M}\frac{\mathrm{d}M}{\mathrm{d}z} = \frac{1}{A_n}\frac{\mathrm{d}A_n}{\mathrm{d}z}. \tag{11}$$

Since that time, considerable effort has been expended in the development of a theoretical understanding of the processes that occur within a magnetic nozzle as well as in the construction of experimental devices.

A recent review [25] covered the most significant aspects of the physics of magnetic nozzles and showed that there are three key processes required for the production of thrust.

1. Plasma must detach from the magnetic field of the nozzle to produce thrust and to prevent damage to the spacecraft by the return of charged particles along the nozzle field lines.
2. Momentum has to be imparted to the spacecraft by the forces on the expelled plasma. The process is mediated by the Lorentz force, the resultant of the sum of the magnetic pressure and the magnetic tension force:

$$\mathbf{F}_t = \mathbf{j} \times \mathbf{B} = -\nabla \frac{\mathbf{B}^2}{2\mu_0} + \frac{1}{\mu_0}(\mathbf{B} \cdot \nabla)\mathbf{B}, \qquad (12)$$

   where the first term on the right corresponds to the isotropic magnetic pressure, the second term corresponds to the magnetic tension force, present only for curved field lines and **j** is the current density.
3. Energy must be transferred from the power supply to the kinetic energy of the propellant.

A later 2D theoretical analysis of the supersonic expansion of a plasma in a diverging magnetic field [26] demonstrated the following.

1. The ambipolar electric field converts the energy of the electrons into directed energy of the ions,
2. A diamagnetic electron Hall current is responsible for the radial confinement and axial acceleration of the plasma. Thrust is the result of the reaction of this current on the currents in the field windings,
3. Prevailing theories for plasma detachment resulting from resistivity, electron inertia and plasma induced magnetic fields are inadequate explanations and detachment relies upon ion inertia and gradual demagnetization.

Overall, these studies demonstrate that incorporating a magnetic nozzle into the design of a plasma thruster makes possible the use of a variety of different plasma sources that by themselves may not efficiently produce a directed high velocity jet.

3.2.3. Electrothermal acceleration. A propellant may be heated and ionized by induction, by radiated energy or by an electrical discharge. The heated propellant is expanded through a magnetic nozzle or through a conventional de-Laval nozzle that converts random thermal energy to directed kinetic energy that provides thrust to the spacecraft.

An approximation of the fully expanded exhaust velocity is given by the following equation that is also employed for chemical rockets:

$$v_e \leqslant \sqrt{2c_p T_c}, \qquad (13)$$

where c_p is the specific heat of the propellant at constant pressure per unit mass and T_c is the maximum temperature that can be sustained by the device [27]. Low molecular weight gases such as hydrogen (H_2 $c_p = 14.32\,\mathrm{kJ\,kg^{-1}\,K^{-1}}$)

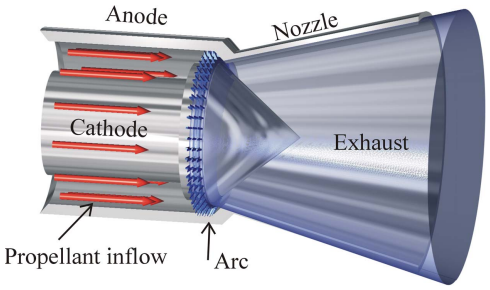

Figure 5. Arcjets are electrothermal thrusters that heat propellant by passing a gas through an arc formed between concentric electrodes. A conventional de-Laval nozzle converts the hot, partially ionized gas to a directed flow that produces thrust that drives the spacecraft.

are the preferred propellants for these sorts of thrusters (figure 5).

3.2.4. Rotating magnetic field (RMF) acceleration. RMF thrusters—also known as ELF or Electrodeless Lorentz Force thrusters—use RMFs to heat and confine plasmas that are then expelled by Lorentz force. The use of RMFs to drive currents in plasmas has been investigated since the 1950 s and is a special case of the more general nonlinear $\mathbf{j} \times \mathbf{B}$ Hall current drive [28]. The RMF is the resultant of the vector sum of two sinusoidally varying components that are 90° out of phase and supplied to antennas that are physically oriented at 90° to each other located outside the axial magnetic field coils. Penetration of the RMF into the plasma drives azimuthal electron currents that reverse the direction of the solenoidal field and result in the formation of an electrically neutral field-reversed closed poloidal field plasmoid that can be accelerated to produce thrust. Since the plasmoid is electrically neutral, an RMF plasma thruster does not require a cathode to produce charge-neutralizing electrons and neither does it require a magnetic nozzle since the plasmoid is accelerated by magnetic repulsion.

The mechanism of plasma confinement and heating in these devices is shown in the following figures (figures 6–8) and described in the following text.

3.2.4.1. RMF plasma current drive mechanism. In this analysis the ions form an immobile, uniformly distributed background of positive charge in which the electrons are regarded as an inertia-less, pressure-less negatively charged fluid.

Given this approximation, the current drive may be understood from the starting point of the generalized Ohm's law [29]:

$$\mathbf{E} = \eta_p \mathbf{j} + \frac{1}{n_e e}(\mathbf{j} \times \mathbf{B}) = \eta_p \left[\mathbf{j} + \frac{\omega_{ce}}{\nu_{ei}}(\mathbf{j} \times \mathbf{e}_B) \right], \qquad (14)$$

where **E** is the electric field strength, η_p is the plasma resistivity, **j** is the current density that has components j_z and j_θ, n_e is the electron number density, e is the electron charge, **B** is the magnetic field vector that has oscillating components B_r and B_θ at the RMF frequency ω_{RMF}, $\mathbf{e}_B$ is the magnetic field unit vector, $\omega_{ce} = \frac{eB}{m_e}$ is the electron cyclotron frequency and

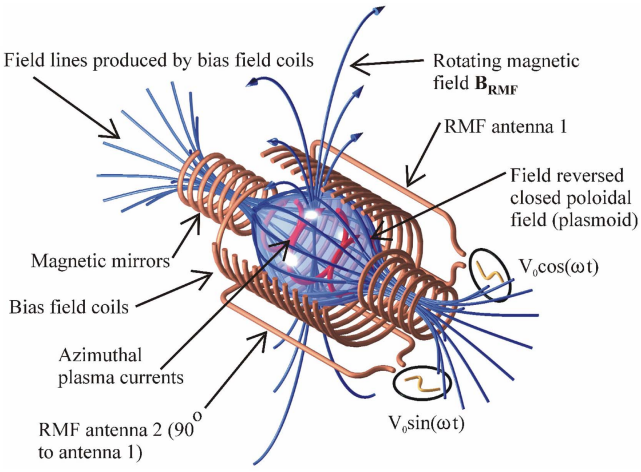

Figure 6. RMF components showing magnetic fields, current drive, azimuthal currents and the field reversed closed poloidal field plasmoid that develops in rotating magnetic field driven plasmas. The figure shows the surrounding confining bias field coil, the two orthogonal antennae that produce a rotating field and the azimuthal plasma currents (red) induced in the plasma by the rotating magnetic field B_{RMF} resulting from AC currents in the RMF antennae. The field coils have been cut away to reveal the plasma and currents.

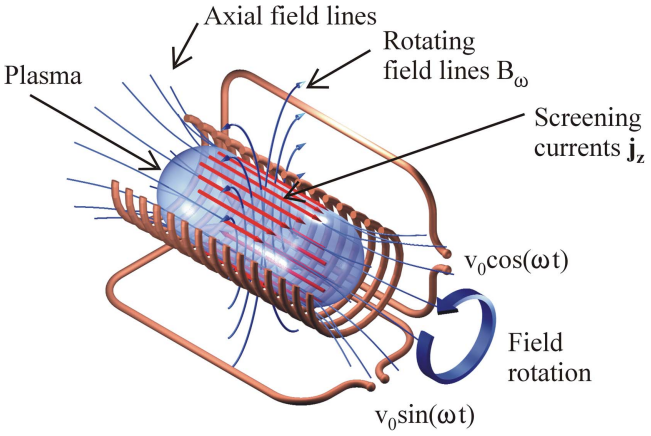

Figure 7. RMF plasma column with screening currents $\mathbf{j}_z$ arising from the induced electric field E_z produced by the application of a rotating magnetic field B_ω where $\frac{1}{n_e e}\mathbf{j}\times\mathbf{B} \ll \eta_p\mathbf{j}$. The effect of the screening currents is to oppose the penetration of the rotating magnetic field into the plasma that drives the electron currents.

$\nu_{ei} = \eta_p \frac{n_e e^2}{m_e}$ is the electron–ion collision frequency where m_e is the electron mass. In this equation $\eta_p\mathbf{j}$ is the resistive term and $\frac{1}{n_e e}(\mathbf{j}\times\mathbf{B})$ is the Hall term.

If the Hall term $\frac{1}{n_e e}\mathbf{j}\times\mathbf{B} \ll \eta_p\mathbf{j}$ then $E_\theta = \eta_p j_\theta = -\frac{d\Phi}{dt}$ is negative and flux leaves the plasmoid and screening currents $\mathbf{j}_z$ arise in the outer layers of the plasma that prevents the RMF from penetrating the plasma (figure 7).

If $\frac{1}{n_e e}\mathbf{j}\times\mathbf{B} \gg \eta_p\mathbf{j}$ and $j_z B_r$ (where the current $\mathbf{j}_z$ is driven by an induced axial electric field produced by the rotating field) is large and negative, then the Hall term has the opposite sign to $\eta_p\mathbf{j}$ and E_θ can be negative. Under those conditions, the flux enters the plasmoid and field reversal

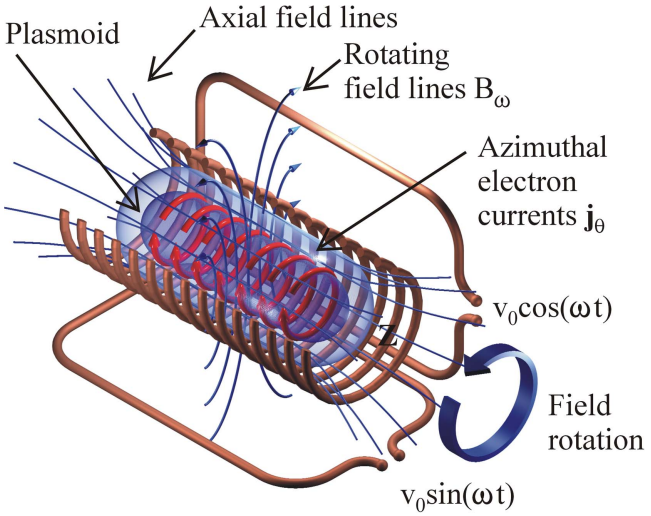

Figure 8. RMF plasma column where $\frac{1}{n_e e}\mathbf{j}\times\mathbf{B} \gg \eta_p\mathbf{j}$ that produces a field reversed plasmoid embedded in the plasma column. The plasmoid is created by the effect of the azimuthal electron currents produced by the rotating magnetic field. The plasmoid forms a separate magnetic domain within the plasma that by a suitable arrangement of magnetic fields can be expelled to produce thrust.

grows, the electrons are magnetized and the rotating field penetrates the plasma producing azimuthal electron currents that create a magnetized plasmoid that forms a reversed field configuration that can be expelled to create thrust (figure 8).

As can be seen from equation (14), $\nu_{ei} \ll \omega_{ce}$ is a requirement if the magnetic field is to penetrate into the plasma while the angular frequency ω_{RMF} of the applied field must be in the range $\omega_{ci} < \omega_{\mathrm{RMF}} < \omega_{ce}$ to ensure that the ions do not co-rotate with the rotating field.

In addition, equation (14) shows that the electron density n_e and the electron–ion collision frequency ν_{ei} determine the extent to which the resistive term dominates the Hall term.

In the absence of plasma, the r and θ components of the rotating field $\mathbf{B}_\omega$ have the form:

$$B_r = B_\omega \cos(\omega t - \theta), \tag{15}$$

$$B_\theta = B_\omega \sin(\omega t - \theta), \tag{16}$$

where B_ω is the amplitude of the rotating field and θ is the azimuthal cylindrical coordinate.

In the presence of plasma the axial components can be determined by introducing the magnetic vector potential A where:

$$\mathbf{B} = \nabla\times\mathbf{A}. \tag{17}$$

And by taking the limit where $\eta_p\mathbf{j} \cong 0$ so that Ohm's law assumes the form:

$$\mathbf{E} = \frac{1}{n_e e}(\mathbf{j}\times\mathbf{B}). \tag{18}$$

It can then be shown that the following equations are exact solutions of Ohm's law:

$$A_z = -B\omega\, r \sin(\omega\, t - \theta), \tag{19}$$

$$B_z = B_{\text{axial}} - \frac{1}{2} ne\omega (r_\text{p}^2 - r^2), \tag{20}$$

where B_{axial} is the axial magnetic field strength and r_p is the plasma diameter.

The azimuthal current density, j_θ is given by:

$$j_\theta = -\frac{1}{\mu_0}\frac{\partial B_z}{\partial r} = -n_\text{e} e \omega_{\text{RMF}} r. \tag{21}$$

This result indicates that the plasma electrons rotate synchronously with the rotating field where the electron drift velocity at any radial position r is given by $r\omega$.

Electromagnetic theory indicates that the RMF will not penetrate the plasma beyond the resistive skin depth δ_s, the distance below the surface of a conductor where the current falls to 0.37 of the surface current. Resistive skin depth is approximated by:

$$\delta_\text{s} = \sqrt{\frac{2\eta_\text{p}}{\mu_0 \mu_\text{r} \omega}}. \tag{22}$$

However when an RMF is applied to a plasma, the electrons rotate with the RMF and in that frame of reference, the RMF appears stationary and the field can penetrate the plasma to the axis of symmetry. In order to penetrate the plasma, the RMF must exceed a threshold value and it has been shown [30] that the RMF magnetic flux density must exceed a value B_ω such that:

$$B_{\omega_{\text{RMF}}} > \sqrt{\frac{\mu_0}{2}}\, en_\text{e} r \sqrt{\eta_\text{p} \omega_{\text{RMF}}}. \tag{23}$$

If the condition is satisfied, the RMF penetrates the plasma and the penetration is maximized when the electrons rotate in synchrony with the rotating field.

3.2.4.2. Thrust produced by the RMF. Thrust produced by the effect of the RMF current drive is similar to that produced by a magnetic nozzle where, independent of the generating mechanism, the induced azimuthal electron current in the presence of the diverging magnetic field creates the axial component of the thrust.

If the radial magnetic field B_r is expressed as $B_\text{r} \cong B_z (r/2R_{\text{coil}})$ and assuming that the electron density is spatially uniform then the thrust can be estimated as:

$$F_\text{t} = L_\text{A} \int_0^{r_\text{p}} j_\theta B_\text{r} (2\pi r) \text{d}r = \frac{\pi\, r_\text{p}}{4R_{\text{coil}}} en_\text{e} L_\text{A} \omega_{\text{RMF}} B_z r_\text{p}^3, \tag{24}$$

where R_{coil} is the axial coil radius, L_A is the length of the accelerating region and r_p is the plasma radius.

For typical values of $\omega_{\text{RMF}} = 6 \times 10^6\,\text{s}^{-1}$, $R_{\text{coil}} \cong r_\text{p} = L_\text{A} = 5\,\text{cm}$, $n_\text{e} = 10^{12}\,\text{cm}^{-3}$, and $B_z = 500\,\text{G}$, equation (24) yields $F_\text{t} = 100\,\text{mN}$ [12].

3.2.5. Rotating electric field (REF) acceleration. The use of REF as a means of accelerating plasma was first reported in 2003 [31]. In this device, a plasma produced by a helicon discharge is electromagnetically accelerated using a REF in the presence of a diverging static magnetic field [32]. The Lissajous thruster consists of a helicon plasma source with two pairs of parallel plates at the outlet energized by sinusoidal voltages with a phase difference of 90° in the same manner as the RMF thruster. The resulting REF induces an azimuthal current in the plasma and the reaction of this current with the radial component of the diverging solenoidal field accelerates the plasma (figure 9).

3.2.5.1. Thrust produced by the REF. Assuming that $R_\text{L} \ll R_\text{G} \ll r_0$, where $R_\text{L} = \frac{v_\perp}{\omega_{\text{ce}}}$ is the Larmor radius, $R_\text{G} = \frac{E_0}{B_z \omega}$ is the gyration radius of electrons moving at the azimuthal cross-field drift velocity under the influence of the REF and $v_{\text{ions}} \ll v_{\text{electrons}}$, the theoretical thrust F_t can be obtained by integrating $j_\theta(r) \times B_\text{r}(r)$ with $B_\text{r}(r) = B_z r/2r_\text{m}$ to give:

$$F_\text{t} = \frac{\pi}{4} e\beta\, n_0\, L_\text{A} \frac{r_0^2}{r_\text{m}} \left(\frac{E_{\text{p0}}^2}{\omega_{\text{REF}} B_z} + \frac{v_\perp m_\text{e}}{e} \right), \tag{25}$$

where e is the electron charge, β is the rate of decline of plasma density, n_0 is the initial electron number density, r_0 is the radius of the thruster, r_m is the radius of the magnetic coil, ω_{REF} is the REF frequency, B_z is the axial magnetic field strength, $v_\perp$ is the plasma perpendicular velocity and E_{p0} is the amplitude of the REF penetration into a uniform magnetized plasma that is given by:

$$E_{\text{p0}} = \left(1 - \frac{1}{\mu_0} \left[\varepsilon_\text{a} - \sqrt{\varepsilon_\text{a}^2 + \mu} \right]^2 \right) \frac{V_0}{2r_0}, \tag{26}$$

where $\varepsilon_\text{a} = 1 - \frac{\omega_{\text{REF}}^2}{\omega_{\text{ce}}^2} \approx 1$, $\mu = \frac{2eV_0 \omega_{\text{pe0}}^2}{m_\text{e} r_0^2 \omega_{\text{ce}}^4}$, V_0 is the amplitude of the REF and ω_{pe0} is the electron plasma frequency.

3.2.6. Acceleration by beating electrostatic waves (BEW). Plasma may be heated by single electrostatic waves (SEW) through a resonant transfer of energy with ions that have a velocity near to the phase velocity of the wave; ion cyclotron heating is a typical example of this mechanism. However, only the small number of ions that have a velocity comparable to the phase velocity absorb energy from the wave by resonant exchange.

Observations of the acceleration of ions in the ionosphere in the late 1970s at an altitude of 1000 km demonstrated that ions could be accelerated by a spectrum of electrostatic waves that propagate orthogonally to a magnetic field provided that there are waves with frequencies separated by an integer multiple of the cyclotron frequency [33].

Subsequent experiments [34] supported that work by showing that a magnetized plasma can be efficiently heated by the interaction of two electrostatic waves in the plasma where the beat frequency between the waves with angular frequencies ω_1 and ω_2 is equal to the ion cyclotron

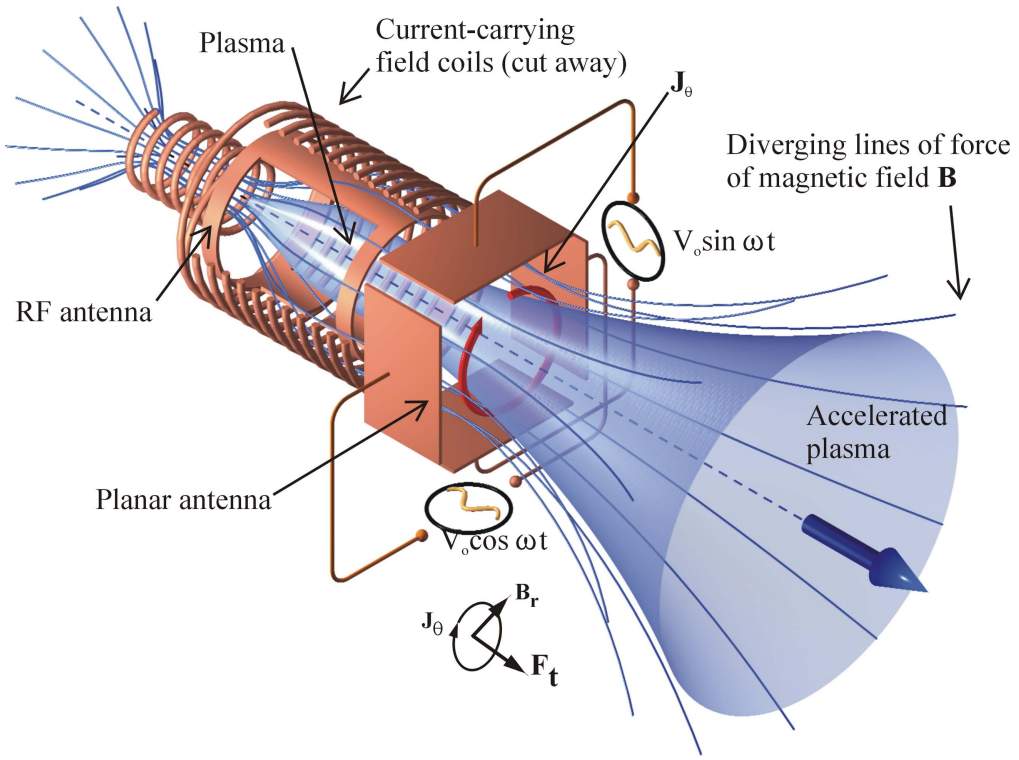

Figure 9. In the Lissajous thruster the rotating electric field created by planar antennae drives an azimuthal current $\mathbf{J}_\theta$ that interacts with the radial component of the solenoid field $\mathbf{B}$ to produce a Lorentz force $\mathbf{F}_t = \mathbf{J}_\theta \times \mathbf{B}_r$ that provides a component of the thrust. Thrust is also produced by the effects of the magnetic nozzle that is formed by the diverging magnetic field.

frequency Ω_{ni}:

$$\omega_2 - \omega_1 = \Omega_{ni}. \tag{27}$$

Plasma heating by BEW is driven initially by the of exchange energy with non-resonant ions that have thermal velocities lower than the phase velocity of the waves. Ions accelerate stochastically until they reach a velocity that is near to the phase velocity of the wave at which point resonant coupling between the wave and ions increases the acceleration of the ions. BEW heating is more effective than SEW heating only if the total wave energy density exceeds a threshold value [35]. Analysis shows that there are distinct regimes of electrostatic wave energy density in which either BEW or SEW will provide superior heating however, since BEW heating accelerates low energy ions, it is an efficient alternative to SEW heating and coupled to a magnetic nozzle, can form a component of an effective electrodeless plasma thruster. Experiments in the Electric Propulsion and Plasma Dynamics Lab at Princeton University have shown that the efficiency of SEW ion heating is ~50% while the efficiency of BEW heating is ~90% [36]. Enhanced heating of ions was observed even though the maximum energy density in that experiment was only 17% of the threshold at which BEW is expected to provide more efficient heating than SEW.

3.2.7. Ponderomotive force thrusters. Ponderomotive force thrusters exploit the nonlinear ponderomotive force $\mathbf{F}_{pf}$ on a charged particle that is proportional to the negative gradient of the intensity of an inhomogeneous oscillating electromagnetic field in the presence of a magnetic field (figure 10). The particle oscillates at the field frequency ω_f and drifts towards the weaker electromagnetic field in a direction that is independent of the polarity of the particle's charge.

3.2.7.1. Thrust produced by the ponderomotive force. In a spatially varying oscillating electric field:

$$\mathbf{E} = \mathbf{E}_0(\mathbf{r}) \cos \omega_f t, \tag{28}$$

where the electric field amplitude $\mathbf{E}_0(\mathbf{r})$ is approximated by:

$$\mathbf{E}_0(\mathbf{r}) = \mathbf{E}_0(\bar{\mathbf{r}}) + \Delta\mathbf{r}(t) \cdot \nabla \mathbf{E}_0(\bar{\mathbf{r}}), \tag{29}$$

where $\bar{\mathbf{r}}$ is the time average over the oscillation period $2\pi/\omega_f$ and $\Delta\mathbf{r}(t)$ is the oscillating component then the ponderomotive force arises along the gradient of $\mathbf{E}_0(\mathbf{r})$ and is given by:

$$\mathbf{F}_{pf} = -\frac{q^2}{4m_e\omega_f^2} \nabla |\mathbf{E}_0(\bar{\mathbf{r}})|^2. \tag{30}$$

In a non-magnetized plasma, the force is directly proportional to the gradient in equation (30) however the force is modified when the oscillating electric field $\mathbf{E}(t)$ has a component perpendicular to an applied magnetic field B and the direction of the force may be determined by the strengths of the electric and magnetic fields (figure 10).

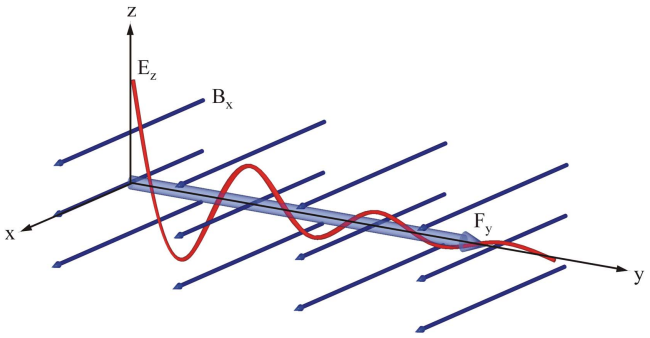

Figure 10. In a ponderomotive force thruster, the force F_y on a charged particle is produced by an inhomogeneous oscillating electromagnetic field of frequency ω_f with an electric field component E_z in the presence of a magnetic field B_x.

In a magnetized plasma the ponderomotive force on an electron is given by:

$$\mathbf{F}_{\text{magnetized}} = -\frac{q^2}{4m_e}\frac{1}{(\omega_f^2 - \omega_{ce}^2)}\frac{\partial E_{0z}^2}{\partial \bar{z}}, \qquad (31)$$

where $\omega_{ce} = \frac{qB}{m_e}$ is the ECR frequency.

In the presence of a magnetic field the direction of the ponderomotive force depends upon the sign of the denominator in equation (31), that is whether $\omega_f^2 > \omega_{ce}^2$ or $\omega_f^2 < \omega_{ce}^2$. This means that the strength of the applied magnetic field and the frequency of the electromagnetic field can be used to control the direction of acceleration and equation (31) shows that the strength of the ponderomotive force is resonantly enhanced when ω_f approaches ω_{ce} (figure 11).

The basic device suffers from two limitations. Firstly, the ponderomotive force primarily accelerates electrons along the magnetic field lines that means that ambipolar acceleration of the ions is necessary to produce thrust, a process that restricts the exhaust velocity. Secondly, the thruster's efficiency may be degraded by detachment losses in the magnetic nozzle that arises in the diverging magnetic field.

A modification of the design that overcomes these problems employs beating electrostatic ion cyclotron waves propagating perpendicularly to the magnetic field that heats the ions and produces a ponderomotive force that acts directly on the ions resulting in an accelerated plasma with a velocity of approximately 20 km s^{-1}, comparable to Hall thrusters [38].

3.2.8. Ponderomotive force thrusters using lasers. The application of intense laser pulses to plasma to produce accelerated particles was first suggested in 1979 [39]. That work showed that as an intense laser pulse propagates through a plasma, a trailing Langmuir wave with a group velocity equal to that of the pulse forms with a longitudinal electric field strength in the range of 1×10^9–1×10^{12} V m^{-1}. That electric field then accelerates charged particles in the plasma (figure 12).

That work demonstrated that an intense electromagnetic pulse can create a wake of plasma oscillations through the action of the nonlinear ponderomotive force. Other studies

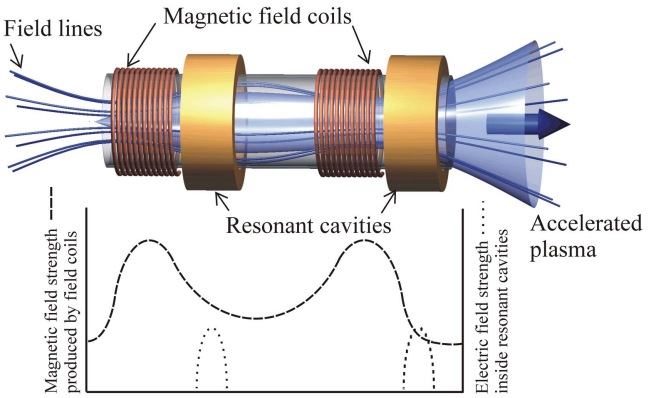

Figure 11. In the microwave driven ponderomotive force thruster the magnetic field windings create a magnetic bottle and a diverging magnetic field. The resonant cavities fed with microwave energy create a localized electromagnetic field with steep gradients that provides the conditions that produce the ponderomotive force acceleration (after [37]).

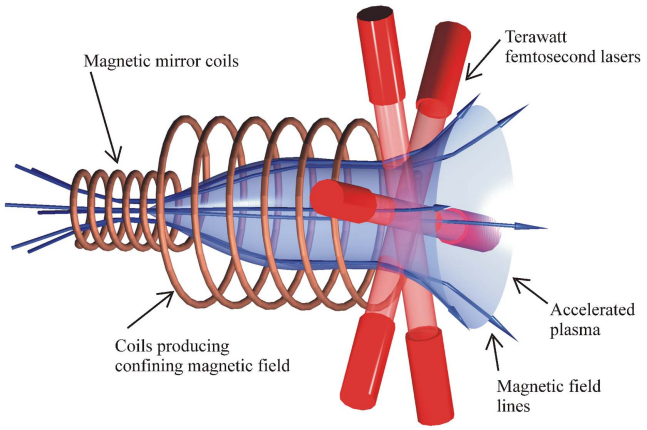

Figure 12. Laser driven ponderomotive force thruster employing femtosecond terawatt pulsed lasers to accelerate plasma confined by an axial magnetic field. A magnetic mirror is used to trap particles that are driven towards the rear of the thruster by the intense electric field produced by the laser pulse. Thrust is produced by the interaction of charged particles with the radial component of the magnetic field.

[40] have shown that there is a presently moderate capacity that a specific impulse of $I_{sp} > 10^3$ s may be achieved with such a device employed as a thruster.

The maximum amplitude of the accelerating wave field is given by [41]:

$$E_{max} = 2.8 \times 10^4 \left(\frac{\lambda_L}{r_L}\right)^2 \frac{P_L}{\lambda_P} \quad 10^9 \text{ V m}^{-1}, \qquad (32)$$

where λ_L is the laser wavelength, r_L is the radius of the laser beam spot size, P_L is the laser power (10^{12} W) and λ_P is the plasma wavelength.

3.2.9. Helicon double layer acceleration. Evidence that charged particles are accelerated in plasmas that contain an electric double layer (EDL) is well established and it is widely accepted that EDLs, in which an electric field arises between two oppositely charged space charge layers, can form in

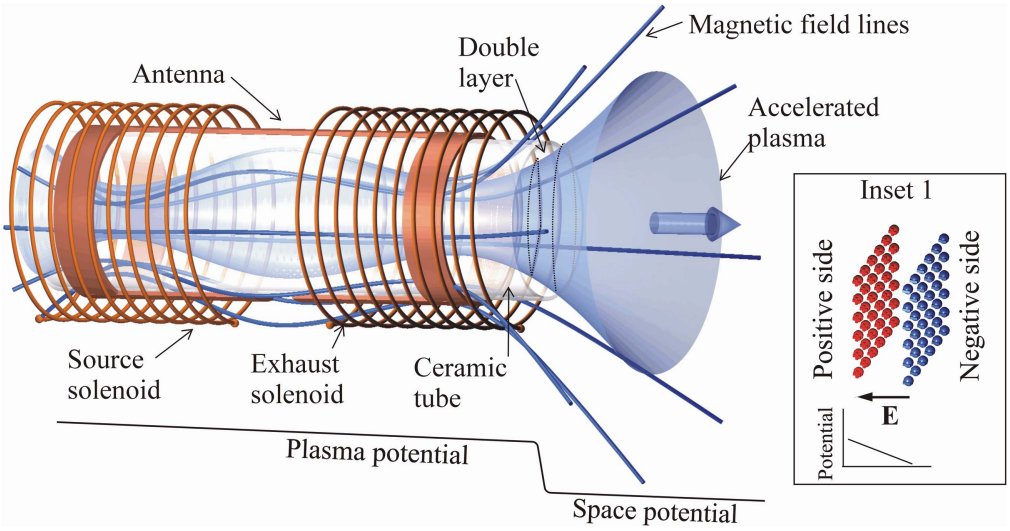

Figure 13. An inductive helicon thruster showing the profile of the axial plasma potential in an expanding plasma containing an electric double layer. Inset 1 shows the structure of the EDL that arises from anisotropies of the pitch angles of ions and electrons in the diverging magnetic field in the expanding plasma.

plasmas. EDLs can form as a result of anisotropies in the pitch angle of ions and electrons in a plasma in a diverging magnetic field [42] and may also be produced by the effect of temperature on the velocities of ions and electrons in an expanding plasma [43]. Separation between the layers is maintained by a balance between electrostatic and inertial forces and the potential difference between the layers is given by $|\Phi_{\mathrm{EDL}}| \geqslant k_{\mathrm{B}} T_{\mathrm{e}}/e$ where k_{B} is Boltzmann's constant and T_{e} is the electron temperature. An EDL is said to be strong if $e\Phi_{\mathrm{EDL}} \gg k_{\mathrm{B}} T_{\mathrm{e}}$.

The acceleration of electrons and ions in such plasmas has been observed in laboratories and astrophysical objects and more recently experimenters have observed the acceleration of ions in a plasma containing a current-free EDL in a helicon discharge [44] (figure 13).

Recent work with an inductive collisionless high-power (900 W) helicon plasma in argon has demonstrated the production of an ion beam that appears to have been accelerated across a double layer like structure that has a time averaged plasma potential difference of 80 V. The ion energy distribution of the beam had a bi-modal Maxwellian form with 77% of the accelerated ions having an energy greater than 65 eV while the energy of the remaining ions peaked at 15 eV, near the plasma potential [45]. Despite that finding, the role of the double layer in the net acceleration of the ions remains under discussion. For instance, the following one-dimensional analysis shows that the net momentum delivered to the plasma by the electric field as it crosses the entire EDL region is zero—assuming that the boundaries of EDLs in real plasmas may have no net charge [46]:

Multiplying the differential form of Gauss's law by the electric field gives:

$$\varepsilon_0 \nabla \cdot \mathbf{EE} = \rho_{\mathrm{n}} \mathbf{E}, \tag{33}$$

where $\mathbf{E}$ is the electric field, ρ_{n} is the net charge density and ε_0 is the permittivity of free space.

In one-dimension the integral form of this equation becomes:

$$\frac{\varepsilon_0}{2}[E(z_2)^2 - E(z_1)^2] = \int_{z_1}^{z_2} \rho_{\mathrm{n}} E \mathrm{d}z. \tag{34}$$

This equation shows that since the electric field at the EDL boundaries (z_1 and z_2) are zero, the electric force on the charge density ρ_{n} is also zero. In an EDL, the force exerted on the ions driven in one direction is balanced by the force exerted on the electrons in the opposite direction and although in an EDL in a divergent magnetic field the magnetic pressure can produce a net force since the EDL is very narrow, that force is negligible [47]. One and two-dimensional studies have shown instead that the acceleration of plasma results from magnetic field pressure arising in a diverging magnetic field that occurs in a magnetic nozzle rather than electrostatic forces in an EDL [46, 48]. Others have suggested that the acceleration of the bulk plasma may be caused by a directed coupling of the plasma electrons with the helicon wave field and the acceleration of the ions by the resulting ambipolar electric field [49] or by a pre-sheath acceleration of ions [50]. A more recent analysis of the processes occurring in current-free EDLs concluded that while the EDLs are produced by the thermodynamic effects of high energy electrons, they make no contribution to the thrust [51].

Even though an EDL may be present in a magnetized plasma, it may not be the only or even the main source of acceleration of ions. Further investigation is required to determine the acceleration mechanism in these thrusters.

3.3. Magnetic mirrors

The simple plasma thruster (figure 1) may be improved by using a magnetic mirror to prevent ions escaping through the sheath to the back wall (figure 14). A magnetic mirror consists of a strongly converging magnetic field as viewed by a particle entering the mirror region. So long as the

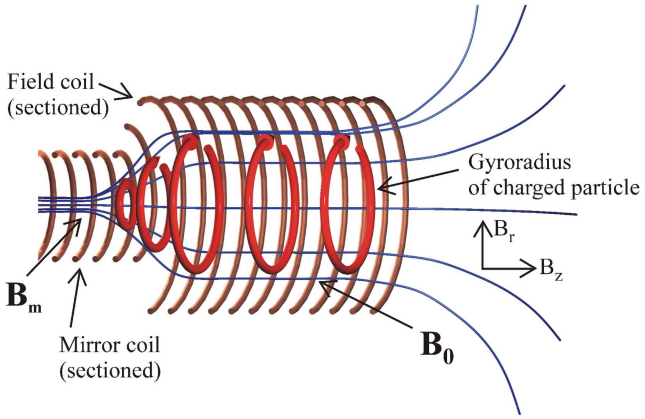

Figure 14. Drift of a particle in a magnetic mirror field $\mathbf{B}_m$ where $\mathbf{B}_0$ = the solenoid flux density. The component B_r gives rise to a force that can trap a particle in a magnetic field through the conservation of the magnetic moment μ_m of the particle.

field gradient $\frac{\partial B_z}{\partial z}$ is almost constant compared to the gyro-radius scale, the magnetic moment of the particle, $\mu_m = \frac{1}{2} m_{ion} v_\perp / B$, is conserved and as the particle's perpendicular velocity $v_\perp$ increases as it moves into a region of stronger magnetic field, the conservation of energy requires that the velocity parallel to the magnetic field $v_{||}$ decreases until it is reflected.

4. Current electrodeless plasma thruster technology development

The development of electrically powered thrusters did not receive serious intention until chemical rockets were able to launch suitable platforms into orbit in the 1960s. Since that time, a plethora of electric propulsion systems have been developed with many either under test or deployed.

In this section we compare the performance of a number of the well-documented electrodeless plasma thrusters on the basis of the following figures of merit that determine the capacity of each type of thruster to enable a specified mission. Those figures of merit are: specific impulse I_{sp} (s), thrust efficiency η_t, thrust F_t (N) and lifetime (h), where available. Figures for the first three figures of merit are commonly available while figures for lifetime of experimental electrodeless thrusters are less so. Despite that limitation, investigators reasonably claim that the absence of electrodes endows their devices with an extended durability because of a reduction in interactions between the plasma and the thruster components [12].

The factors that limit the achievement of high exhaust velocities v_e and resulting high specific impulse I_{sp} in chemical propulsion systems are firstly the enthalpy of the propellants and secondly the maximum temperature that the materials of the rocket combustion chamber and nozzle can withstand. Electric propulsion systems overcome the enthalpy constraint by imparting more energy into a unit mass of the propellant, and in electrodeless thrusters and magnetically shielded Hall thrusters, the material temperature constraint is overcome by the use of magnetic fields that isolate the thruster structure from sputtering by the ionized propellant. Much higher specific impulses and consequently greatly reduced fuel consumption may be achieved compared to a chemical rocket. To date, all deployed plasma thrusters have used electrodes. Since those thrusters have been devices with power supplies that deliver at most a few kilowatts, for example the 25 cm Xenon Ion Propulsion System (XIPS-25) [52], erosion of the electrodes has not caused significant problems and nor has the space charge limited thrust density of approximately 440 N m^{-2} for gridded ion thrusters been an impediment [53].

As missions require more powerful thrusters, electrode erosion will become an important consideration, one that can be answered by magnetic shielding or by electrodeless designs. Electrodeless designs do not have thrust density limits, are less sensitive to propellant purity and commonly do not require a charge neutralizer. To date (2017), no electrodeless plasma thrusters have been used in operational spacecraft although the design and construction of prototypes of various devices has been an active area of investigation for decades. The following discussion examines the electrodeless plasma thrusters that have been realized or have been shown by the number of publications to be devices of considerable interest.

Table 3 summarizes typical specific impulse, thrust efficiencies and thrusts of some deployed and developing electric thrusters. Note that the highest specific impulse for chemical thrusters (H_2–O_2) is limited to approximately 450 s [54].

4.1. RMF thrusters

4.1.1. The electrodeless Lorentz force (ELF) thruster. The ELF thruster (figure 15) uses a RMF to produce a plasmoid using the RMF drive mechanism where the plasmoid is driven from the thruster by $j_\theta \times B_r$ forces produced either by a conical magnetic field gradient or by sequencing currents in an array of flux coils [64]. Since the magnetic field of the plasmoid is closed, detachment of the plasmoid from the thruster magnetic field is complete and as the plasmoid is uncharged, charge neutralization of the departing plasmoid is not required.

4.1.2. Lorentz force on the plasmoid in the ELF thruster. The plasmoid in the ELF thruster is subject to a constant acceleration by the magnetic field produced by the conical solenoid that surrounds the plasma. Studies of various propellants show that RMF acceleration contributes 80% of the directed kinetic energy of the thruster while thermal expansion accounts for 16%. The thrust efficiency, η_t, for a 30 kW thruster when operating on water or 95% carbon dioxide mixed with 2% nitrogen and 3% argon is calculated from measurements and approximations and reported to be 85 +% [65]. A later study of a sample return mission from the minor planet Ceres with a similar device (ELF-160A) gives a thrust efficiency of 60% when operating on xenon for the outbound voyage to Ceres and a thrust efficiency of 55% when using water obtained from Ceres for the inbound voyage to Earth [66].

4.1.3. Erosion of walls in the ELF thruster. In experiments where the ELF thruster was fired for 3000 discharges no

Table 3. Specific impulses, thrust efficiencies and thrusts of electric thrusters, deployed and experimental.

Thruster type	Electrodes	I_{sp} (s)	Thrust efficiency η_t	Thrust	Reference
Pulsed plasma	Y	240–760	20%–30%	1×10^{-4} Ns	[55]
Gridded ion	Y	7650	77%	0.43 N	[56]
Hall	Y	1600	50%–60%	$(2.5–12) \times 10^{-3}$ N	[57]
Magneto-plasma-dynamic	Y	3670	38.8%	$\sim 250 \times 10^{-3}$ N	[58]
Mini helicon	N	1000–4000	~20%	$\sim 10 \times 10^{-3}$ N	[59]
Inductively heated arcjet (TIHTUS)	Y	2000	29%	6.0 N	[60]
Pulsed inductive	N	5500	50%	7.5×10^{-2} Ns	[61]
Hybrid (VASIMR)	N	3400	56%	3.6 ± 0.2 N	[62]
Electron cyclotron resonance	N	429 (Xe)	3.5%	0.86×10^{-3} N	[63]
Electrodeless Lorentz force (ELF)	N	1000–6000	50+%	1.0 N (average)	[64]

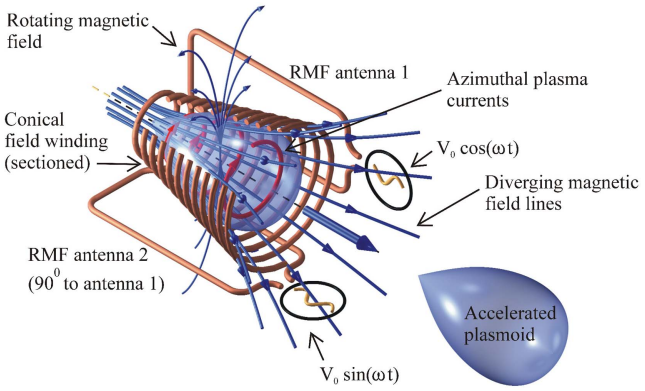

Figure 15. ELF rotating magnetic field thrusters expel a field reversed plasmoid that is accelerated by the Lorentz force produced by a conical solenoid surrounding the plasma. The diverging magnetic field acts as a magnetic nozzle that further accelerates the plasmoid and converts a proportion of the thermal energy of the plasma into directed kinetic energy that propels the spacecraft [64]. The performance of this device is shown in table 4.

erosion of the thruster walls were detected [67]. While these measurements suggest that erosion of components in ELF thrusters is not likely to be a life-limiting factor in the operation of these devices, much longer duration testing is required to verify that claim.

4.1.4. Current status of ELF thrusters. Although the original intent of the development of ELF thrusters was to produce a working fusion rocket and reactor [68], that goal has now receded and instead, a practical thruster that uses a RMF driven from an external power supply to heat and accelerate a plasma has been produced [64]. Table 4 shows reported values for the figures of merit. Other work on ELF thrusters has been aimed at optimizing the geometry and materials of the RMF antennae and improving the plasma loading whilst reducing unwanted resistive coupling [69].

4.1.5. RMF thrusters with a helicon plasma source. The helicon electrodeless advanced thruster project has investigated the use of RMFs and an alternating axial magnetic field to accelerate plasma produced by a helicon plasma source [70] (figure 16).

In the RMF experiment, the RMF is generated by pairs of coils that are supplied with AC currents that have a phase

Table 4. Reported performance parameters for an ELF thruster [64].

Parameter	Measured value
Specific impulse I_{sp} (s)	1000–6000 (N_2, air and Xe)
Thrust efficiency η_t	50+%
Thrust (N)	Up to 1.0 mNs per impulse bit
Lifetime (h)	Not stated

difference of 90°. An azimuthal plasma current j_θ produced by the effect of the RMF reacts with the radial component of the axial field to produce thrust through the Lorentz force $F_t = j_\theta \times B_r$. The RMF was found to accelerate the plasma by 19% compared to the plasma velocity produced by a simple helicon plasma thruster [71].

In the $m = 0$ mode in a helicon plasma the current density is at a maximum at the center of the RF coil and has azimuthal symmetry, an obvious advantage in a thruster. When an AC current is applied to the $m = 0$ coil that is coaxial with the axial field coil, it generates an alternating axial magnetic field that, through Faraday's law, induces an azimuthal plasma current j_θ that reacts with the radial component of the axial field to produce thrust in alternating axial directions. The thrust produced by one-half cycle accelerates the plasma out of the thruster, the accelerated plasma produced by the opposite half cycle collides with the rear wall of the discharge tube.

4.2. REF thrusters (Lissajous thrusters)

Measurements of the performance of an experimental thruster that used a REF in an expanding magnetic field to accelerate plasma that had been produced by a helicon source have found that the thrust–if any–produced by the REF was below the noise signal generated by the thrust stand. Although a theoretical analysis of the Lissajous plasma accelerator indicated that such a device could produce a specific impulse of 10 000, in practice the measured performance has been much less promising [72].

A later study found that the REF produced a thrust of 4.95 μN and concluded that such a value was not useful for practical applications [32].

Those experimental results show a weak dependence of the ion velocity as a function of the phase difference of the

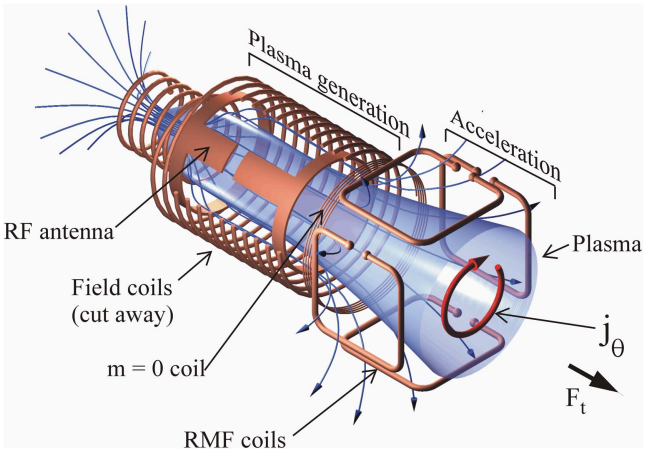

Figure 16. Helicon plasma source with an RMF accelerator (after [70]). The performance of this device is shown in table 5.

Table 5. Reported best performance parameters for a helicon plasma source with an RMF and an $m = 0$ accelerator.

Parameter	Measured value	
Specific impulse I_{sp} (s)	Argon	2000
	Xenon	1500
Power efficiency η_P (mN kW^{-1})	Argon	8.3
	Xenon	16
Thrust (mN)	Argon	21
	Xenon	41

voltages applied to the antenna plates. That result indicated a very small electromagnetic acceleration of the plasma and it is considered that most of the power is consumed in ionizing and heating the plasma while the plasma acceleration is mainly due to expansion of the plasma through the magnetic nozzle formed in the diverging field.

4.3. Pulsed inductive plasma accelerators (PIT)

Pulsed inductive plasma accelerators are spacecraft propulsion devices that store energy in a capacitor and produce thrust by coupling that energy into a propellant by induction from a rising current in a coil that is in close proximity to the propellant [73]. In some devices the electric field that arises from the time varying magnetic field according to Faraday's law $\left(E = -\frac{d\Phi}{dt}\right)$ ionizes the propellant. In others, the propellant is ionized separately but in both cases the Lorentz force between an induced plasma current and the magnetic field produced by the coil current accelerates the ionized propellant.

Two inherent physical effects have obstructed the development of efficient devices. Firstly, any delay in the ionization of the propellant means that instead of coupling into the ionized gas, energy is dissipated in the coil. Secondly, the maximum amount of energy has to be transferred into the ionized gas before it is driven away from the face of the coil since the coupling between the coil and the ionized gas is a function of mutual inductance that is strongly determined by their separation. The effect is quantified by the Lovberg criterion [74] that states that the thrust efficiency η_t of pulsed inductive thrusters is limited by the ratio of the total change in circuit inductance ΔL to the initial circuit inductance L_0. That is:

$$\eta_t \leqslant \frac{\Delta L}{L_0}. \tag{35}$$

The ratio $\frac{\Delta L}{L_0}$ is maximized when the plasma forms as closely as practical to the surface of the inductor without causing damage to the coil.

The delay in ionization may be addressed by pre-ionizing the propellant with a separate mechanism since pre-ionization permits current sheet formation at lower voltages and discharge energies than in pulsed inductive thrusters that rely solely upon a rapidly changing magnetic field to ionize the propellant. The effect of declining mutual inductance as the plasma sheet moves away from the coil is not so easily resolved and remains a limitation [53].

In investigations dating back to the 1960s and 70s planar devices were constructed that had thrust efficiencies that ranged from 5% (20 cm coil, $I_{sp} = 1200$ s) to 18% (30 cm coil, $I_{sp} = 1470$ s). Larger devices developed in the 1980 s were found to have greater thrust efficiencies and specific impulse (1 meter coil, $\eta_t = 42\%$ at $I_{sp} = 1540$ s and $\eta_t = 50\%$ at $I_{sp} = 2240$ s) [75]. Further investigations using a thrust stand revealed that the figures for the specific impulse and thrust efficiency for the larger device that were calculated from measurements of current density and magnetic fields were overstated by 24% and 42% respectively. Since that time engineering developments such as increasing the rate of current rise (dI/dt) and the replacement of spark-gap switches with solid-state devices have led to significant improvements in the performance of these thrusters although up until 2011 the PIT Mark Va developed in the early 1990s remained the most efficient and best performing pulsed inductive thruster ($\eta_t = 55\%$, $I_{sp} = 6000$ s [73]) (table 6).

More recent developments that utilize ion cyclotron resonance ionization of the propellant at the face of a conical theta pinch coil are intended to improve the thrust efficiency of these devices [76]. Interestingly, a recently developed model [77] that produced a qualitative agreement with results from tests of the PIT Mk V thruster showed that the optimum coil angle is 90°, that is, a flat plate although a PIT with a coil angle of 60° may have some advantages in propellant utilization that could compensate for any loss in electrical transfer efficiency.

4.3.1. Planar pulsed inductive thrusters without pre-ionization. PIT thrusters without pre-ionization utilize a single inductive coil for both plasma generation and electromagnetic acceleration (figure 17①) [80]. Capacitors deliver a current pulse to the primary coil windings that through Faraday's law ionizes the propellant at the same time as it is injected across the face of the coil (figure 17②). The reaction between the magnetic field in the coil and the plasma current generates a Lorentz force ($\mathbf{F}_t = \mathbf{J}_{plasma} \times \mathbf{B}_{field}$) that

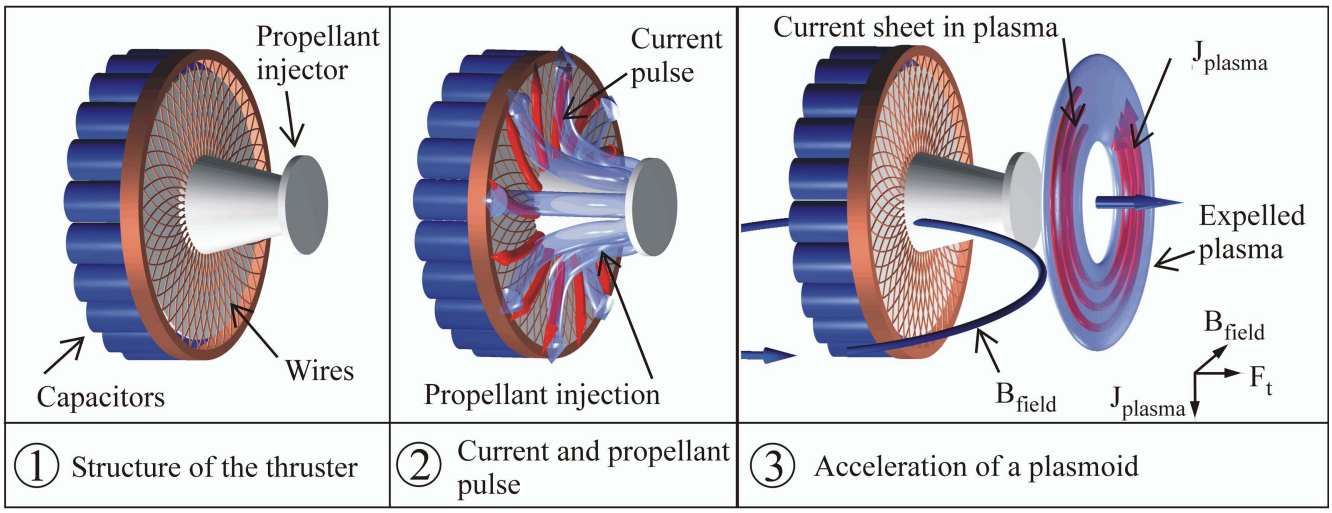

Figure 17. Operation of a typical planar pulsed inductive thruster without pre-ionization. Gaseous propellant is ionized by the electric field produced by the rapidly changing magnetic field and the resulting plasma is driven from the thruster by the Lorentz force. The performance of several devices of this design are shown in table 6.

Table 6. Examples of reported performance parameters for PIT thrusters.

Thruster	I_{sp} (s)	Thrust efficiency η_t	Energy (J) per pulse	Reference
Plasmoid thruster experiment (PTX)	500–4300	0.4%–49%	280	[78]
30 cm PIT[a]	1470	18%	675	[73]
1 m PIT	1236	25.4%	4840	[73]
PIT Mk 1 (NH_3)	1360 (worst)	21.3%	4840	[74]
	2766 (best)	31.9%	5760	
PIT Mk Va (NH_3)	6000	~55%	~4000	[73]
PIT Mk VI	2750	18.9%	4050	[73]
Conical theta pinch PIT	1500 to >4500 (Ar), 1000–2500 (Xe)	5% (single pulse)	500	[79]

[a] Values calculated from field measurements are probably an overestimate.

expels the plasma producing a thrust that propels the spacecraft (figure 17③).

4.3.2. Planar pulsed inductive thrusters with pre-ionization. The Faraday acceleration with radio-frequency assisted discharge (FARAD) thruster developed in 2004 is a PIT that typically uses argon as a propellant, although water vapor, Ne, He, Kr, H_2, O_2, CO_2, Cl, F and Xe are also possible propellants (figure 18).

The propellant is ionized by a helicon discharge and the resulting plasma then guided by a magnetic field to flow radially outwards across the face of an inductive coil. In operation, a large azimuthal current, J_{coil}, is pulsed through the coil at a rate $\frac{dJ_{coil}}{dt} \geqslant 10^{10}$ A s^{-1}.

A current pulse of this magnitude induces a current sheet in the plasma and the induced azimuthal current J_{plasma} in the current sheet interacts with the applied magnetic field, B_{field}, resulting in a Lorentz body force, $J_{plasma} \times B_{field}$ on the plasma.

The resulting force has two components, $j_\theta B_r$ which is axial and accelerates the plasma, and $j_\theta B_z$ which is radial and confines the plasma thereby minimizing damage to the surrounding wall of the thruster.

Thrust is produced by the Lorentz force between the magnetic field produced by the coil current and the induced plasma current sheet [81].

Reports of the performance of a 100 J per pulse FARAD laboratory thruster have been disappointing. Figures for thrust and thrust efficiency were not reported and the stated reasons for this outcome were that most of the propellent was not ionized sufficiently for the coil currents to couple to the plasma or was too far from the coil face. In addition, the current sheet was not magnetically impermeable which also reduced the acceleration of the propellant [82].

Later designs have employed an electrodeless ECR preionization scheme that, by a suitable arrangement of permanent magnets, produce a seed plasma which is further ionized by a current pulse through the inductive coil. By employing ECR pre-ionization, microwave assisted discharge inductive plasma accelerators reduce the need for high voltages and a current rise-time sufficient to ionize the cold propellant [76].

4.3.3. Conical PIT thrusters. The single stage FARAD [80] thruster (SS-FARAD) consists of a single conical antenna coil through which both the ionization and acceleration pulse is

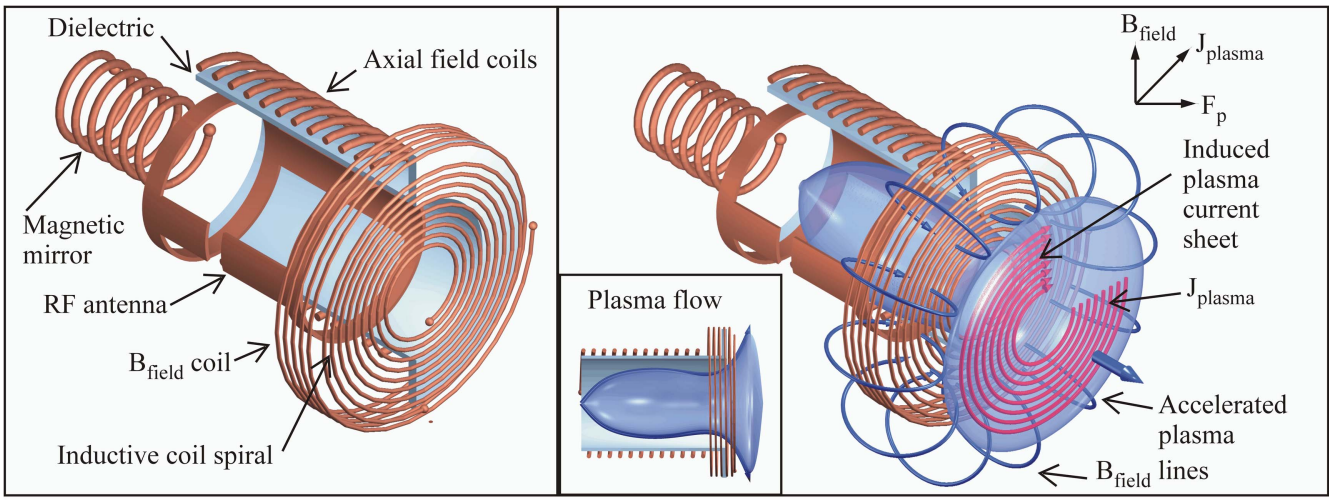

Figure 18. FARAD (Faraday acceleration with radio-frequency assisted discharge) thruster that uses the $\mathbf{j} \times \mathbf{B}$ force developed by the interaction between an induced plasma current, J_{plasma} produced by a changing current J_{coil} in the spiral inductive coil and a magnetic field, B_{field} produced by the B field coil. The magnetic pressure pushes the plasma away from the coil. The performance of this device is discussed in the preceding text (after [81]).

applied to the gaseous propellant. The SS-FARAD thruster eliminates external magnetic fields as well as secondary antennas required for plasma generation and other components required for ionization so is lighter and less complex than previous designs, significant advantages for a compact spacecraft thruster. Recent results indicate that thrusters of this type with smaller conical angles produce greater thrust in contradiction to the predictions of a previous model [83]. Initial measurements made on a conical thruster with a half angle of 20° and an applied voltage of 5 kV produced a maximum impulse of 0.097 mNs with an argon flow rate $90 < \dot{m} < 150$ mg s^{-1}. The investigators suggested that the low thrust of these devices was attributable in part to a large inductive voltage drop in the transmission line from the capacitors to the coil. Other possibilities were a premature current sheet decoupling caused by radial current sheet motion or by an initially radially-displaced current sheet formation point in the thruster.

4.3.4. Lifetime limits in the PIT thruster. The limited available evidence suggests that the lifetime of thrusters that use induction to accelerate plasmas is not limited by erosion of electrodes and contamination of other spacecraft components by the products of erosion. Failure of semiconductor devices used to switch large currents may occur before erosion by sputtering causes significant damage to the electrodes.

4.4. Helicon thrusters

Helicon thrusters consist of a helicon-type antenna providing energy to a plasma source attached to a magnetic nozzle that transforms the randomized thermal energy of the plasma into directed kinetic energy (figure 19).

In simple helicon-type thrusters, a significant part of the thrust is produced by plasma pressure that develops against the back wall of the thruster. Energy is lost from the plasma to the back wall of the thruster through the sheath and the

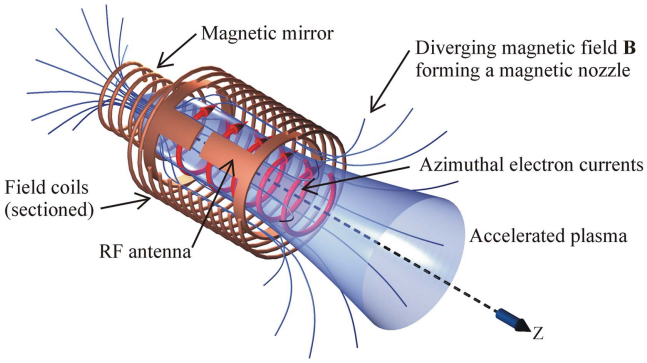

Figure 19. Generalized helicon type thruster showing the principal components: (1) the field coils that produce the magnetic field **B** that forms the confining field and the magnetic nozzle and (2) the helicon antenna, usually placed inside the field coils, that supplies the RF power that provides the energy to the generate the plasma from the propellant. The plasma is accelerated by the magnetic nozzle described in section 3.2.2. A magnetic mirror prevents plasma from flowing out of the rear of the plasma source.

bombardment of the back wall by the plasma causes damage by sputtering as well as a reduction in the thrust efficiency η_t. Since nearly all of the energy supplied to the thruster is consumed in ionizing the propellant, losses to the back wall are nearly equal to that lost to the plasma expelled from the exit, effectively halving the thrust efficiency. Plasma confinement by magnetic mirrors (section 3.3) is well understood and is an effective means of reducing plasma losses to the back wall and improving the thrust efficiency of a radio frequency heated plasma thruster.

The relatively low ion temperature of 0.3 eV produced by helicon-type sources [32] is another factor that reduces the effectiveness of simple helicon-type thrusters since, being effectively an electrothermal thruster, the specific impulse is proportional to the square root of the plasma energy and therefore its temperature. In the absence of other means of

Table 7. Summary of prototype helicon-type thrusters ([84] and others). η_m is the propellant utilization efficiency. Values are given where available.

Prototype	I_{sp} (s)	η_t (%)	Thrust	η_m (%)	Power	Reference
Mini helicon thruster experiment (mHTE)	1000–4000	18–20	10 mN	90	700–1100 W	[59]
Helicon plasma hydrazine combined micro (HPHCOM)	1200	13	1.5 mN	90	50 W	[85]
	422	13	0.5 mN	—	8 W	[86]
Permanent magnet expanding plasma (PMEP)	500	1	3 mN	<50	700 W	[87]
High power helicon thruster (HPHT)	4750 (H_2)	—	—	—	30 kW	[88]
Helicon double layer thruster (HDLT)	280	ℂ1	1–2.8 mN	—	250–650 W	[89]
Permanent magnet helicon plasma thruster (PM-HPT)	2000	7.5	15 mN	—	2 kW	[90]

accelerating the plasma, the specific impulse I_{sp} of approximately 200 s is not an improvement on chemical rockets [15].

A recent review [84] has summarized the performance of representative helicon-type thruster prototypes and highlighted the design parameters. Table 7 is an extract from that paper with some additions.

4.4.1. Helicon double layer thruster (HDLT). In 2003 a group at the Australian National University, following earlier work [91], reported that an EDL that formed in a plasma in a diverging magnetic field appeared to produce an ion beam, useful as a thruster [44] (figure 20).

An RF antenna that was wave coupled to the propellant gas produced the plasma. The graph shows the step in the plasma potential created either by an electrical double layer [44] or by a pre-sheath acceleration of ions [50].

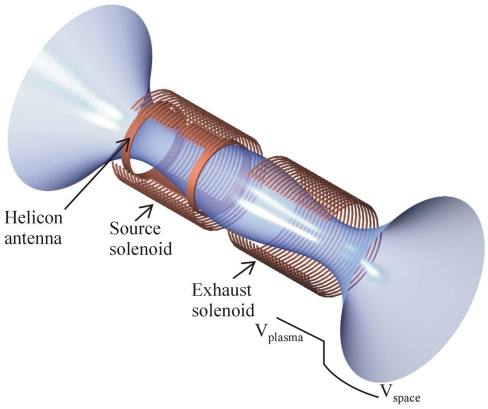

Figure 20. Helicon double layer plasma thruster showing the main components of the ANU experiment. The field coils have been cut away to reveal the helicon antenna and the plasma.

4.5. Hybrid thrusters

VASIMR is an example of a hybrid thruster that uses a helicon plasma source, ion cyclotron resonance heating and a magnetic nozzle to respectively ionize, heat and accelerate plasma [92] (figure 21).

4.6. Plasma thrusters using traveling waves in a transmission line

Plasma can be accelerated by the Lorentz force associated with a moving magnetic field produced by traveling waves of voltage and current that propagate along transmission lines when either a pulse of current or a source of alternating current is applied to one end of the line. In either case, the propagation velocity is given by:

$$v_p = 1/\sqrt{LC}, \tag{36}$$

where L and C are respectively the inductance and capacitance of the elements of the line (figure 22).

In most systems the propagation velocity is of the order of 10^4–10^5 m s^{-1} [93].

Transmission line accelerators using helium as a propellant were investigated in the 1960s [94] however those were high power (160 kW) devices that employed large currents to generate a magnetic field strength sufficient to accelerate plasma in a water cooled thruster tube. A slightly later investigation [95] reported lower efficiencies that were ascribed to the fact that the device was limited to operating at a much lower power (13 kW) since the accelerator tube was not water cooled. In those experiments, the greatest thrust efficiency (7.5%) was obtained when operating with argon as a propellant when the accelerator length corresponded to a ¼ wavelength of the RF input whereas when xenon was used the greatest thrust efficiency (6%) was obtained with an accelerator length of one wavelength. The specific impulse obtained with argon was 2200 s and for xenon, 1200 s.

A low power device developed in a more recent investigation [96] uses either an ion cyclotron resonance or helicon plasma source to produce an argon plasma. The plasma is accelerated by propagating magnetic fields with velocities from 5000 to 25 000 m s^{-1} that are produced by pulses applied to a sequentially switched series of coils at a repetition rate of 5 Hz. The energy of the pulses delivered to each coil was 0.014 J and the overall power was 9.8 W.

An interaction between the plasma and the propagating magnetic field has been observed however, no measurements of specific impulse, thrust efficiency or thrust have yet been published.

4.7. Plasma thrusters using a HiPIMS ion source with a magnetic nozzle

The development of high power impulse magnetron sputtering discharge technology (HiPIMS) [97, 98] together with improvements in the understanding of the physics of magnetic nozzles [99] encouraged this investigation into the combination

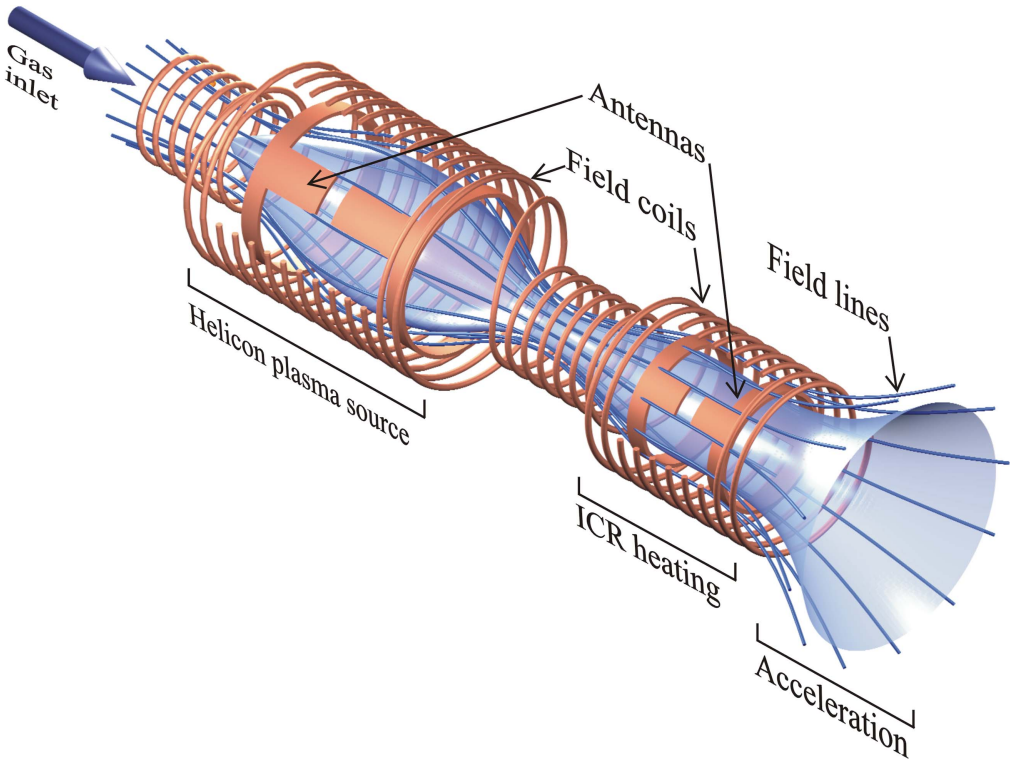

Figure 21. Hybrid electro-thermal thruster that uses a helicon plasma source, ion cyclotron heating of the resulting plasma and a magnetic nozzle to accelerate the heated plasma in the diverging magnetic field lines. The field coils have been cut away to reveal the antennas that supply radio frequency energy to ionize the propellant and then heat and accelerate the resulting plasma.

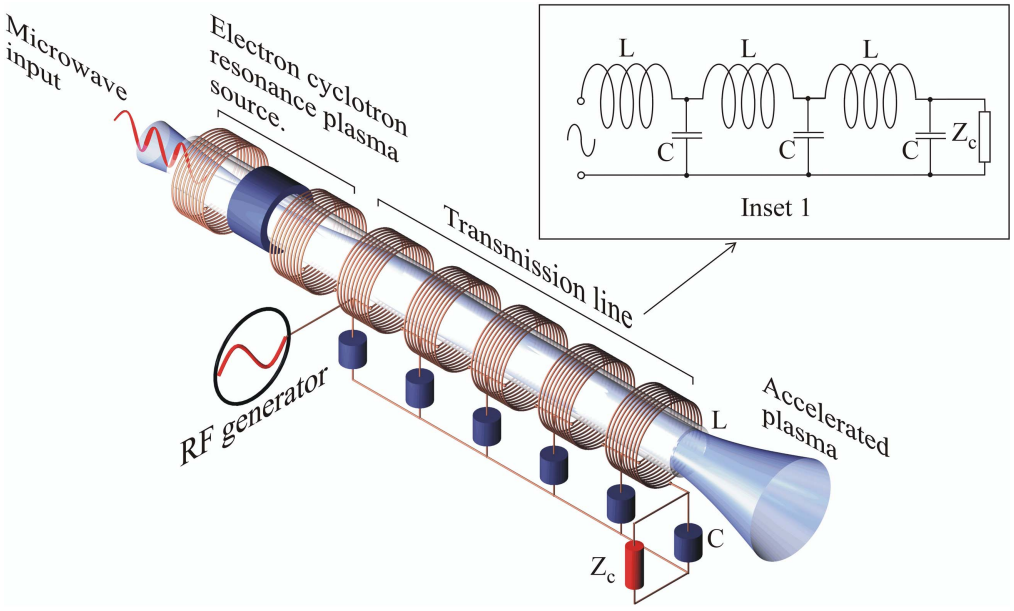

Figure 22. Traveling wave plasma accelerator. Plasma, generated for instance by an electron cyclotron resonance source, is accelerated by the traveling axial magnetic field produced by the waves that propagate along the transmission line when alternating current or a current pulse is fed into the line. To prevent reflections of the waves, the transmission line has to be terminated with a characteristic impedance Z_c (inset 1).

of these devices with the intention of producing a thruster with greater internal efficiency and thrust than existing solid propellant plasma thrusters.

The HiPIMS thruster (figure 23, from [100]) utilizes ions of target material and has no electrodes that may be subject to ion bombardment (other than the metallic propellant mass). Copper was used in this device since it known to support self-sputtering [101] although self-sputtering was not achieved in the device tested. That is, once sputtering has been initiated either with a pulse of gas or with a laser, the process will continue to produce thrust without the need to re-start sputtering and importantly for a spacecraft, the thruster will

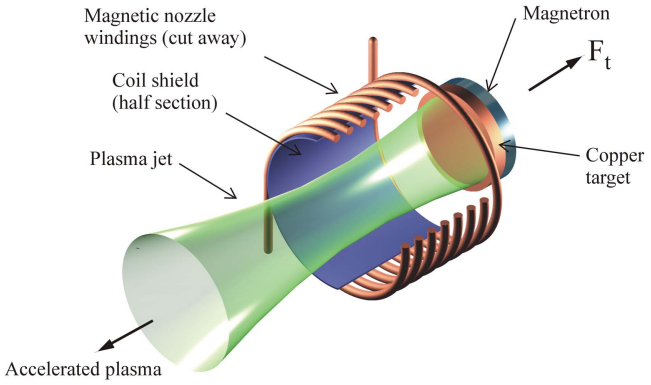

Figure 23. A HiPIMS plasma source located at one end of a current-carrying solenoid produces ions and electrons that are accelerated by the diverging magnetic field that exists at the ends of a solenoid.

Table 8. Measured performance of a HiPIMS copper ion thruster [100].

Parameter	Measured value
Specific impulse I_{sp} (s)	1543 (copper)
Thrust efficiency η_t	6%
Thrust (N) @ input power	3.77 μN@3.6 kW

operate continuously in a high vacuum. At high power intensities the density of the sputtered copper atoms is so great that a considerable number of copper atoms are ionized by collisions with plasma electrons. These copper ions are accelerated by the cathode voltage and sputter the copper target even in a vacuum [102]. The emission of ions and electrons from the magnetron source is initiated by bombardment of the target with argon ions from a pulse of gas that is energized by a high intensity current pulse. Thrust F_t is produced by the acceleration of copper ions by the Lorentz force in the magnetic nozzle that are expelled from the target (table 8).

5. Summary and conclusions

Electric thrusters of various kinds have been developed over the last 60 years and while their advantages in propellant mass and specific impulse are obvious for interplanetary missions, until recently the majority have been employed for near Earth applications such as station keeping for geosynchronous communications satellites. Only three interplanetary missions have used plasma thrusters as their primary propulsion, all gridded ion: Deep Space 1 [5]; Hayabusa [103] and Dawn [6]. Smart-1 was a lunar orbiter that used a PPS-1350-G Hall thruster with a specific impulse of 1540 s [104].

In 2010 solar electric propulsion (SEP) was regarded as suitable for 15 of the 28 missions considered for NASA's Planetary Decadal Survey [105]. A Hall thruster with a specific impulse in the range of 2500–3000 s was seen as capable of meeting the requirements of those 15 missions and a commercially available device that could meet the specifications was identified. Further developments such as magnetic shielding have been shown to effectively eliminate wall erosion as a failure mode in Hall thrusters by orders of magnitude in devices operating at a specific impulse of 3000 s [106]. As an outcome of such successful demonstrations, NASA's Space Technology Mission Directorate SEP Technology Demonstration Mission is funding the development of a 12.5 kW magnetically shielded Hall thruster as a propulsion system for future missions [107]. High-power Hall thrusters have reached a state of development where they have become the device of choice for the majority of foreseeable missions that could use SEP and 20–50 kW Hall thrusters to support human exploration missions are under development [108].

So far, conventional chemical rockets have propelled missions to Mars on relatively slow Hohmann transfer orbits that would expose crews to hazardous cosmic radiation [109]. SEP has been proposed as a means of delivering cargo to Mars orbit yet even with high-thrust chemical propulsion, crews would still endure transit times that would extend into 6 months or more [110].

Minimizing transit time requires a high-energy propulsion system such as the proposed VASIMR thruster that, operating at a power of 12 MW with an initial mass of 100 tonnes and an I_{sp} of 5000 s, could deliver a crew to Mars in 3 months. Taking approximately half the time of the chemically propelled NASA Design Reference Mission (DRM) that has a comparable initial mass, such a mission could be accomplished with a moderate technical advance required to develop space nuclear power generators with a specific mass $<4\,\mathrm{kg\,kW^{-1}}$ [111]. Calculations indicate that a 50 MW VASIMR could reach Mars in 39 days assuming an appropriate planetary alignment.

Table 9 lists the performances of the electrodeless and electrodeless thrusters discussed in the previous sections.

Extended testing of the integrated VX-200SS VASIMR prototype is intended to bring that device to Technological Readiness Level of 5 (TRL-5) where the assembled components are tested in a near-realistic environment. Despite that development, it is evident from table 9 that the ELF Thruster has the greatest potential for near-term deployment since even though the specific mass of the thruster may have been reduced by the effect of scaling, it is approximately half that of VASIMR and an order of magnitude better than the PIT, devices that have similar specific impulses. In addition, unlike VASIMR, the ELF does not have losses associated with plasma detachment from the nozzle field. The success of this device suggests that thrusters that expel plasmoids without the complications of detachment have an advantage over those that employ magnetic nozzles.

The development of the ELF has resulted in a useful device while progress in developing new forms of the pulsed inductive thruster with greater thrust efficiency have been hampered by difficulties in understanding the physics of those devices. That concern is exemplified by the results of tests of conical PIT thrusters while a recently published model has shown that the most thrust efficient PIT thruster is similar to the original flat plate devices and suggests that attempts to improve conical PITs will prove difficult although the conical

Table 9. Representative summary of the performance of the most significant plasma thrusters either operational or under development with values for the most important parameters that are given where available.

Thruster	I_{sp} (s)	Thrust efficiency η_t	Thrust (mN)	Thrust/power (mN kW^{-1})	Specific mass kg kW^{-1}	Reference
			Electrodeless thrusters			
Electrodeless Lorentz force thruster (ELF)	1000–6000	50+%	Up to 1.0 mNs per impulse bit	35–95	0.7 scaled to 200 kW	[16]
Pulsed inductive thruster (PIT) Mk Va	6000	55%	0.4 mNs per impulse bit	—	8.1	[74]
Conical theta pinch PIT	4500 (Ar), 2500 (Xe)	5% (single pulse)	1.5 mNs (Ar) per impulse bit	—	—	[79]
VASIMR VX-200	5000	60%	5000	25	1.5 (scaled from a MW level device)	[16]
Helicon plasma hydrazine combined micro	422	13%	0.5	62.5	—	[86]
			Thrusters with electrodes			
Gridded ion (XIPS-25) high power	3550 (avg.)	68.8%	165	38.4	0.093	[52]
Hall NASA-457M cluster	3000	63%	8400	42	1.3 (thruster)	[16]
Magneto-plasma-dynamic (2D AF-MPDT Iwakata)	1000–5000	31.5%	1720	4.7	—	[112] (I_{sp}), [113] (other parameters)
Radio frequency ion thruster (RIT 15)	3000	55%	30	39	—	[114]
Arcjet 1 kW H_2–N_2	~600	~42%	~170	200	—	[115]

PITs may have some advantages in propellant utilization efficiency.

A similar device, the pulsed plasmoid thruster (PTX), achieves a thrust efficiency approaching that of the ELF although it is still in an early stage of development. Considering its similarity to conical PITs, the high thrust efficiency claimed for that device needs to be confirmed.

Much effort has been expended in the development of helicon thrusters that have the attraction of simplicity yet the low plasma temperature of those devices continues to impede their development although some improvement in thrust efficiency has been achieved by adding an acceleration stage to the outlet of the device at the cost of increased complexity. The EDL that forms in plasma in diverging magnetic fields was initially believed to be responsible for the acceleration of plasma yet an analysis has shown that the increase in velocity in plasma in the HDLT is more likely caused by the effect of the magnetic nozzle that forms in the diverging field. Recent work with high power helicon plasmas has demonstrated the formation of a double layer that apparently produced an ion beam with energies in excess of 65 eV suggests that the double layer is responsible for at least some fraction of the observed acceleration. More work is required to establish these devices as useful thrusters.

Other electrodeless thruster mechanisms—such as traveling wave accelerators—may prove practical however much work will be required before those devices are able to challenge the most developed technologies.

Extended lifetime measurements are still required for most electrodeless designs however the absence of electrodes that may be subject to erosion and the preliminary data available suggests that high power (MW) electrodeless plasma thrusters will predominate as mission durations extend and power levels increase. Magnetically shielded high-power Hall thrusters are also being developed.

While the advent of a fusion rocket would remove electric thrusters from the role of primary thrust producers, until that time electric thrusters will continue to displace chemical thrusters for satellite station keeping and for interplanetary missions requiring a high specific impulse [116].

Acknowledgments

The financial support of the Australian Research Council for this project is acknowledged. The Australian Government is acknowledged for the provision of an Australian Postgraduate Award.

References

[1] Thomson J J 1897 *Phil. Mag.* **44** 293
[2] Choueiri E Y 2004 *J. Propul. Power* **20** 193
[3] Sovey J S, Rawlin V K and Patterson M J 2001 *J. Propul. Power* **17** 517
[4] Kazeev M N, Kozubskiy K N and Popov G A 2009 Victor Khrabrov—pioneer of the first space electric propulsion system development and space tests *Proc. 31st Int. Electric Propulsion Conf. (Ann Arbor, MI)* IEPC-2009-235
[5] Marcucci M G and Polk J E 2000 *Rev. Sci. Instrum.* **71** 1389
[6] Brophy J 2011 *Space Sci. Rev.* **163** 251
[7] Polzin K A 2007 Scaling and systems considerations in pulsed inductive thrusters *Proc. 30th Int. Electric Propulsion Conf. (Florence, Italy)* IEPC-2007-192
[8] Chang-Diaz F R and Yang T F 1987 Plasma-gas interaction studies in a hybrid plume plasma rocket *Annual Report, 1 Sep. 1986–30 Aug. 1987* (Cambridge, MA: Plasma Fusion Center, Massachusetts Institute of Technology)
[9] Squire J P *et al* 2016 Advances in duration testing of the VASIMR® VX-200SSTM system *Proc. 52nd AIAA/SAE/ASEE Joint Propulsion Conf. (Salt Lake City, UT)*
[10] Rafalskyi D and Aanesland A 2016 *Plasma Sources Sci. Technol.* **25** 043001
[11] Mazouffre S 2016 *Plasma Sources Sci. Technol.* **25** 033002
[12] Shihara S *et al* 2014 *IEEE Trans. Plasma Sci.* **42** 1245
[13] Garrigues L and Coche P 2011 *Plasma Phys. Controlled Fusion* **53** 124011
[14] Ahedo E 2011 *Plasma Phys. Controlled Fusion* **53** 124037
[15] Cohen S A *et al* 2006 *IEEE Trans. Plasma Sci.* **34** 792
[16] Brown D L, Beal B E and Haas J M 2010 Air Force Research Laboratory high power electric propulsion technology development *Proc. 2010 IEEE Aerospace Conf. (Big Sky, MT)*
[17] Rovey J L and Gallimore A D 2008 *J. Propul. Power* **24** 1361
[18] de Grys K, Mathers A and Welander B 2010 Demonstration of 10 400 h of operation on 4.5 kW qualification model hall thruster *Proc. 46th AIAA/ASME/SAE/ASEE Joint Propulsion Conf. & Exhibit (Nashville, TN)* AIAA 2010-6698
[19] Gorshkov O A *et al* 2007 Development of high power magnetoplasmadynamic thrusters in the USSR *Proc. 30th Int. Electric Propulsion Conf. (Florence, Italy)* IEPC-2007-136
[20] Fruchtman A 2008 *IEEE Trans. Plasma Sci.* **36** 403
[21] Erckmann V and Gaspari U 1994 *Plasma Phys. Controlled Fusion* **36** 1869
[22] LaPointe M R 2000 Theta-pinch thruster for piloted deep space exploration *Proc. 36th AIAA/ASME/SAE/ASEE Joint Propulsion Conf. and Exhibit (Las Vegas, NV)* AIAA paper 2000-3365
[23] Arefiev A V and Breizman B N 2008 *Phys. Plasmas* **15** 042109
[24] Andersen S A *et al* 1968 *Phys. Lett.* **27** 527
[25] Ebersohn F H *et al* 2012 Magnetic nozzle plasma plume: review of crucial physical phenomena *Proc. 48th AIAA/ASME/SAE/ASEE Joint Propulsion Conf. & Exhibit (Atlanta, GA)* AIAA 2012-4274
[26] Martínez M M 2013 Analysis of magnetic nozzles for space plasma thrusters *PhD Thesis* Universidad Politécnica de Madrid, Madrid, Spain
[27] Jahn R G and Choueiri E Y 2002 Electric propulsion ed R A Myers *Encyclopedia of Physical Science and Technology* 3rd edn (San Diego, CA: Academic) p 128
[28] Jones I R 1999 *Phys. Plasmas* **6** 1950
[29] Slough J T and Miller K E 2000 *Phys. Plasmas* **7** 1945
[30] Hoffman A L *et al* 2006 *Phys. Plasmas* **13** 012507
[31] Toki K *et al* 2003 Preliminary investigation of helicon plasma source for electric propulsion applications *Proc. 28th Int. Electric Propulsion Conf. (Toulouse, France)* IEPC 03-0168
[32] Nakamura T *et al* 2012 *Trans. JSASS Aerospace Tech. Japan* **10** Tb_17
[33] Bénisti D, Ram A K and Bers A 1998 *Phys. Plasmas* **5** 3224
[34] Vail P J and Choueiri E Y 2013 Experimental characterization of plasma heating with beating electrostatic waves at high wave energy density *Proc. 33rd Int. Electric Propulsion Conf. (Washington, DC)* IEPC-2013-204
[35] Jorns B and Choueiri E Y 2012 Experimental characterization of plasma heating with beating electrostatic waves *Proc.*

48th AIAA/ASME/SAE/ASEE Joint Propulsion Conf. & Exhibit (Atlanta, GA) AIAA-2012-4194
[36] Jorns B and Choueiri E Y 2009 Experiment for plasma energization with beating electrostatic waves *Proc. 31st Int. Electric Propulsion Conf. (Ann Arbor, MI)* IEPC-2009-199
[37] Emsellem G D and Larigaldie S 2007 Development of the electrodeless plasma thruster at high power: investigations on the microwave-plasma coupling *Proc. 30th Int. Electric Propulsion Conf. (Florence, Italy)* IEPC-2007-240
[38] Jorns B and Choueiri E Y 2011 Thruster concept for transverse acceleration by the beating electrostatic waves ponderomotive force *Proc. 32nd Int. Electric Propulsion Conf. (Wiesbaden, Germany)* IEPC-2011-214
[39] Hooker S M 2013 *Nat. Photon.* **7** 775
[40] Williams G J Jr 2007 Spacecraft propulsion utilizing ponderomotive forces (The Ohio Aerospace Institute)
[41] Williams G J Jr and Gilland J H 2009 *AIP Conf. Proc.* **1103** 175
[42] Alfvén H and Falthammar C G 1963 *Cosmical Electrodynamics* 2nd edn (London: Oxford University Press)
[43] Block L P 1978 *Astrophys. Space Sci.* **55** 59
[44] Charles C and Boswell R 2003 *Appl. Phys. Lett.* **82** 1356
[45] Sung Y T, Li Y and Scharer J E 2016 *Phys. Plasmas* **23** 092113
[46] Fruchtman A 2006 *Phys. Rev. Lett.* **96** 065002
[47] Fruchtman A and Makrinich G 2009 Plasma sources as thrusters *Proc. 31st Int. Electric Propulsion Conf. (Ann Arbor, MI)* IEPC-2009-197
[48] Takahashi K *et al* 2011 *Phys. Rev. Lett.* **107** 235001
[49] Ziemba T *et al* 2005 High power helicon thruster *Proc. 41st AIAA/ASME/SAE/ASEE Joint Propulsion Conf. and Exhibit (Tucson, AZ)* AIAA 2005-4119
[50] Chen F F 2006 *Phys. Plasmas* **13** 034502
[51] Ahedo E and Sánchez M M 2008 The role of current-free double-layers in plasma propulsion *Proc. 44th AIAA/ASME/SAE/ASEE Joint Propulsion Conf. & Exhibit (Hartford, CT)* AIAA 2008-5005
[52] Goebel D M *et al* 2009 Evaluation of 25 cm XIPS© thruster life for deep space mission applications *Proc. 31st Int. Electric Propulsion Conf. (Ann, Arbor, MI)* IEPC-2009-152
[53] Jahn R G 2006 *Physics of Electric Propulsion* (Mineola, NY: Dover)
[54] Rapp D C 1990 High energy-density liquid rocket fuel performance *Proc. 26th Joint Propulsion Conf. (Orlando, FL)* AIAA-90-1968
[55] Molina-Cabrera P, Herdrich G, Lau M and Fausolas S 2011 Pulsed plasma thrusters: a worldwide review and long yearned classification *Proc. 32nd Int. Electric Propulsion Conf. (Wiesbaden, Germany)* IEPC-2011-340
[56] Patterson M J, Pinero L and Sovey J S 2009 Near-term high power ion propulsion options for earth-orbital applications *Proc. 45th AIAA/ASME/SAE/ASEE Joint Propulsion Conf. & Exhibit (Denver, CO)* AIAA 2009-4819
[57] Smirnov A, Raitses Y and Fisch N J 2002 *J. Appl. Phys.* **92** 5673
[58] Krülle G, Auweter-Kurtz M and Sasoh A 1998 *J. Propul. Power* **14** 754
[59] Batishchev O V 2009 *IEEE Trans. Plasma Sci.* **37** 1563
[60] Böhrk H and Auweter-Kurtz M 2006 High power space propulsion system TIHTUS—an overview *Proc. 57th Int. Astronautical Congress (Valencia, Spain)* IAC-06-C4P406
[61] Polzin K A and Reneau J P 2009 *IEEE Trans. Plasma Sci.* **37** 359
[62] Longmier B W *et al* 2011 *J. Propul. Power* **27** 915
[63] Jarrige J *et al* 2013 Performance comparison of an ECR plasma thruster using argon and xenon as propellant gas *Proc. 33rd Int. Electric Propulsion Conf. (Washington, DC)* IEPC-2013-420
[64] Slough J, Kirtley D and Weber T 2009 Pulsed plasmoid propulsion: the ELF thruster *Proc. 31st Int. Electric Propulsion Conf. (Ann Arbor, MI)* IEPC-2009-265
[65] Kirtley D *et al* 2012 Steady operation of an FRC thruster on Martian atmosphere and liquid water propellants *Proc. 48th AIAA/ASME/SAE/ASEE Joint Propulsion Conf. & Exhibit (Atlanta, GA)* AIAA 2012-4071
[66] West M D, Charles C and Boswell R W 2010 *J. Propul. Power* **26** 892
[67] Kirtley D *et al* 2011 Pulsed plasmoid propulsion: air-breathing electromagnetic propulsion *Int. Electric Propulsion Conf.* IEPC-2011-015
[68] Miller K, Slough J and Hoffman A 1998 *AIP Conf. Proc.* **420** 1352
[69] Waldock J, Kirtley D and Slough J 2013 Electromagnetic optimization of FRC-based pulsed plasma thrusters *Proc. 33rd Int. Electric Propulsion Conf. (Washington, DC)* IEPC-2013-376
[70] Kuwahara D *et al* 2015 High-density helicon plasma thrusters using electrodeless acceleration schemes *Presented at Joint Conf. of 30th Int. Symp. on Space Technology and Science, 34th Int. Electric Propulsion Conf. and 6th Na-satellite Symp. (Hyogo-Kobe, Japan)* IEPC-2015-386/ISTS-2015-B-386
[71] Furuawa T *et al* 2016 *Int. J. Phys. Math. Sci.* **3** 518
[72] Matsuoka T *et al* 2011 Progress in development for helicon plasma thrusters by use of the rotating electric field (Lissajous acceleration) *Proc. 32nd Int. Electric Propulsion Conf. (Wiesbaden, Germany)* IEPC-2011-079
[73] Polzin K A 2011 *J. Propul. Power* **27** 513
[74] Dailey C L and Lovberg R H 1993 The PIT MkV pulsed inductive thruster *NASA Contractor Report* 191155 Lewis Research Centre Under Contract NAS 1-19291
[75] Lovberg R H and Dailey C L 1981 Large inductive thruster performance measurement *AIAA/JSASS/DGLR 15th Int. Electric Propulsion Conf. (Las Vegas, NV)* Paper 81-0708
[76] Hallock A K and Polzin K A 2010 Design of a microwave assisted discharge inductive plasma accelerator *Space Propulsion (San Sebastian, Spain, 3–6 May 2010)* SP-2010-1842709
[77] Martin A K 2016 *J. Phys. D: Appl. Phys.* **49** 025201
[78] Eskridge R H and Martin A K 2007 Progress on the PT-1 prototype plasmoid thruster *AFRL Space Propulsion and Power Workshop (Washington, DC)*
[79] Hallock A K *et al* 2015 *IEEE Trans. Plasma Sci.* **43** 433
[80] Feldman M S and Choueiri E Y 2011 Single stage faraday accelerator with radio-frequency assisted discharge (SS-FARAD) *Presented at the 32nd Int. Electric Propulsion Conf. (Wiesbaden, Germany)* IEPC-2011-220
[81] Choueiri E Y and Polzin K A 2004 Faraday accelerator with radio-frequency assisted discharge (FARAD) *Proc. 40th AIAA/ASME/SAE/ASEE Joint Propulsion Conf. and Exhibit (Fort Lauderdale, FL)* AIAA paper 2004-3940
[82] Polzin K A, Rose M F and Miller R 2008 Laboratory-model integrated-system FARAD thruster *Proc. 44th AIAA/ASME/SAE/ASEE Joint Propulsion Conf. (Hartford, CT)* AIAA 2008-4821
[83] Hallock A K *et al* 2012 Effect of inductive coil geometry on the operating characteristics of an inductive pulsed plasma thruster *Proc. 48th AIAA/ASME/SAE/ASEE Joint Propulsion Conf. & Exhibit (Atlanta, GA)* AIAA paper 2012-3928
[84] Navarro-Cavallé J N *et al* 2013 Helicon plasma thrusters: prototypes and advances on modelling *Presented at the 33rd Int. Electric Propulsion Conf. (Washington, DC)* IEPC-2013-285
[85] Pavarin D *et al* 2008 Feasibility study of medium-power helicon thruster *Proc. 44th AIAA/ASME/SAE/ASEE Joint Propulsion Conf. & Exhibit (Hartford, CT)* AIAA 2008-4927

[86] Trezzolani F *et al* 2013 Low power radio-frequency plasma thruster development and testing *Proc. 33rd Int. Electric Propulsion Conf. (Washington, DC)* IEPC-2013-153
[87] Takahashi K *et al* 2011 *Appl. Phys. Lett.* **98** 141503
[88] Ziemba T, Slough J and Winglee R 2005 *AIP Conf. Proc.* **746** 965
[89] Pottinger S *et al* 2011 *J. Phys. D: Appl. Phys.* **44** 235201
[90] Takahashi K *et al* 2013 *J. Phys. D: Appl. Phys.* **46** 352001
[91] Hairapetiat G and Stenzel R L 1991 *Phys. Plasmas* **3** 899
[92] Squire J P *et al* 2016 Advances in duration testing of the VASIMR® VX-200SS system *Proc. 52nd AIAA/SAE/ASEE Joint Propulsion Conf. (Salt Lake City, UT)* AIAA 2016-4950
[93] Fabris A L and Caelli M A 2013 Traveling magnetic field plasma accelerator *Proc. 33rd Int. Electric Propulsion Conf. (Washington, DC)* IEPC-2013-86
[94] Heflinger L, Ridgway S and Schaffer A 1965 *AIAA J.* **3** 1028
[95] Palmer R W and Jones R E 1967 Experimental investigation of a variable-length constant velocity travelling magnetic wave plasma accelerator *NASA Technical Note* TN D-4205 (Washington, DC: National Aeronautics and Space Administration)
[96] Feraboli S, Fabris A L and Cappelli M A 2015 Experimental setup for the development of a traveling magnetic field plasma accelerator *Joint Conf. of 30th Int. Symp. on Space Technology and Science, 34th Int. Electric Propulsion Conf. and 6th Na-Satellite Symp. (Hyogo-Kobe, Japan)* IEPC-2015-442p/ISTS-2015-b-442p
[97] Kouznetsov V *et al* 1999 *Surf. Coat. Technol.* **122** 290
[98] Gudmundsson J T *et al* 2012 *J. Vac. Sci. Technol.* A **30** 030801
[99] Takahashi K *et al* 2014 *Plasma Sources Sci. Technol.* **23** 044004
[100] Bathgate S N *et al* 2016 *Eur. Phys. J. Appl. Phys.* **76** 30801
[101] Anders A and Andersson J 2008 Sputtering in vacuum: a technology for ultraclean metallization and space propulsion *Proc. 23rd Int. Symp. on Discharges and Electrical Insulation in Vacuum (Bucharest, Romania)*
[102] Kukla R *et al* 1990 *Vacuum* **41** 1968
[103] Yoshikawa M, Fujiwara A and Kawaguchi J 2006 *Proc. Int. Astron. Union* **2** (14) 323–4
[104] Koppel C R and Estublier D 2005 The SMART-1 hall effect thruster around the Moon: in flight experience *Proc. 29th Int. Electric Propulsion Conf. (Princeton, NJ)* IEPC-2005-119
[105] Hofer R R 2010 High-specific impulse operation of the BPT-4000 hall thruster for NASA science missions *Proc. 46th AIAA/ASME/SAE/ASEE Joint Propulsion Conf. & Exhibit (Nashville, TN)* AIAA 2010-6623
[106] Hofer R R *et al* 2013 Wear test of a magnetically shielded hall thruster at 3000 s specific impulse *Proc. 33rd Int. Electric Propulsion Conf. (Washington, DC)* IEPC-2013-033
[107] Kamhawi H *et al* 2014 Overview of the development of the solar electric propulsion technology demonstration mission 12.5 kW hall thruster *Proc. 50th AIAA/ASME/SAE/ASEE Joint Propulsion Conf., AIAA Propulsion and Energy Forum (Cleveland, OH)* AIAA 2014-3898
[108] Polk J E *et al* 2011 An overview of NASA's electric propulsion programs, 2010-11 *Proc. 32nd Int. Electric Propulsion Conf. (Wiesbaden, Germany)* IEPC-2011-330
[109] Cucinotta F A *et al* 2014 *Life Sci. Space Res.* **2** 54
[110] Percy T, McGuire M and Polsgrove T 2015 Combining solar electric propulsion and chemical propulsion for crewed missions to Mars *IEEE Aerospace Conf. (Big Sky, MT)*
[111] Ilin A V *et al* 2011 VASIMR® human mission to Mars *Space, Propulsion & Energy Sciences Int. Forum (College Park, MD)*
[112] Lev D and Choueiri E Y 2010 Scaling of efficiency with applied magnetic field in mangnetoplasmadynamic thrusters *Proc. 46th AIAA/ASME/SAE/ASEE Joint Propulsion Conf. & Exhibit (Nashville, TN)* AIAA 2010-7024
[113] Iwakawa A, Nakata D and Kuninaka H 2009 Performance of two-dimensional applied-field magneto-plasma-dynamic thruster *Proc. 31st Int. Electric Propulsion Conf. (Ann Arbor, MI)* IEPC-2009-226
[114] Leiter H J, Loeb H W and Schartner K H 1999 RIT15S and RIT 15 LP—the development of high performance mission optimized ion thrusters *Proc. 35th Joint Propulsion Conf. and Exhibit (Los Angeles, CA)* AIAA-99-2444
[115] Pan W X, Huang H J and Wu C K 2010 *Plasma Sci. Technol.* **12** 473
[116] Cassibry J *et al* 2015 *J. Spacecr. Rockets* **52** 595